JCI The Journal of Clinical Investigation

# Differential aortic aneurysm formation provoked by chemogenetic oxidative stress

Apabrita Ayan Das, … , Taylor A. Covington, Thomas Michel

*J Clin Invest.* 2025. https://doi.org/10.1172/JCI188743.

Research In-Press Preview Cardiology Vascular biology

## Graphical abstract

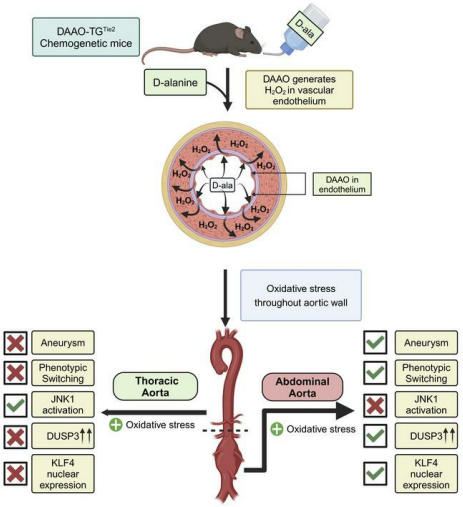

# Differential aortic aneurysm formation provoked by chemogenetic oxidative stress

Apabrita Ayan Das[1,2], Markus Waldeck-Weiermair[1,2,3], Shambhu Yadav[1,2], Fotios Spyropoulos[1,2,4],Arvind Pandey[1,2], Tanoy Dutta[1,2], Taylor A. Covington[1,2] and Thomas Michel*[1,2]

**Affiliations:**
1. Cardiovascular Medicine Division, Brigham and Women's Hospital, Boston, MA, USA
2. Harvard Medical School, Harvard University, Boston, MA, USA.
3. Molecular Biology and Biochemistry, Gottfried Schatz Research Center, Medical University of Graz, Graz, Austria.
4. Department of Pediatrics, Brigham and Women's Hospital, Boston, MA, USA.

***Corresponding Author:**
**Name:** Thomas Michel
**e-mail:** thomas_michel@hms.harvard.edu
**Address:** Cardiovascular Medicine Division, Brigham and Women's Hospital, Harvard Medical School, Harvard University, Boston, MA, USA.

**Conflict of Interest:**

The authors have declared that no conflict of interest exists

**Keywords:**

Oxidative stress, Aneurysm, Chemogenetics, Vascular Biology

**Abstract:**

Aortic aneurysms are potentially fatal focal enlargements of the aortic lumen; the disease burden disease is increasing as the human population ages. Pathological oxidative stress is implicated in development of aortic aneurysms. We pursued a chemogenetic approach to create an animal model of aortic aneurysm formation using a transgenic mouse line DAAO-TG$^{Tie2}$ that expresses yeast D-amino acid oxidase (DAAO) under control of the endothelial Tie2 promoter. In DAAO-TG$^{Tie2}$ mice, DAAO generates the reactive oxygen species hydrogen peroxide ($H_2O_2$) in endothelial cells only when provided with D-amino acids. When DAAO-TG$^{Tie2}$ mice are chronically fed D-alanine, the animals become hypertensive and develop abdominal but not thoracic aortic aneurysms. Generation of $H_2O_2$ in the endothelium leads to oxidative stress throughout the vascular wall. Proteomic analyses indicate that the oxidant-modulated protein kinase JNK1 is dephosphorylated by the phosphoprotein phosphatase DUSP3 in abdominal but not thoracic aorta, causing activation of KLF4-dependent transcriptional pathways that trigger phenotypic switching and aneurysm formation. Pharmacological DUSP3 inhibition completely blocks aneurysm formation caused by chemogenetic oxidative stress. These studies establish that regional differences in oxidant-modulated signaling pathways lead to differential disease progression in discrete vascular beds, and identify DUSP3 as a potential pharmacological target for the treatment of aortic aneurysms.

## Introduction

Elevated levels of reactive oxygen species (ROS) in the vasculature have long been linked to hypertension and aortic aneurysm formation associated with pathological oxidative stress (1–7). It is unclear whether oxidative stress plays a causal role in the development of hypertension or aortic aneurysms, or whether oxidative stress is instead merely associated with these complex disease states. Many of the current animal models of aortic aneurysm formation and hypertension are hampered by methodological complexities, and yet other models may not replicate the molecular mechanisms implicated in disease progression in humans (8, 9). Here we used a chemogenetic approach (10, 11) to develop an animal model that leverages a key feature shared by many of the disease states that lead to hypertension and aneurysm formation: oxidative stress in the vasculature.

Chemogenetic approaches utilize recombinant proteins that are selectively activated by unique ligands or substrates to elicit specific responses in target cells (12). Intracellular redox balance can be dynamically regulated using chemogenetic approaches exploiting a recombinant yeast D-amino acid oxidase (DAAO) that can be activated to generate hydrogen peroxide ($H_2O_2$(12). Yeast DAAO is a stereospecific enzyme that generates $H_2O_2$ as part of its catalytic scheme involving the oxidation of D-amino acids to their corresponding α-keto acids; here, we use D-alanine as the DAAO substrate (10, 11, 12). In addition to producing $H_2O_2$, DAAO generates equimolar ammonia and pyruvate, but the intracellular concentrations of these other DAAO products are much higher than $H_2O_2$ levels; thus, cellular levels of ammonia (13) and pyruvate are not substantively affected by DAAO catalysis (14). Most mammalian tissues contain L- but not D-amino acids, so the recombinant DAAO is inactive until D-alanine is provided to cells expressing DAAO. We previously generated and characterized transgenic mouse lines that express DAAO under control of tissue-specific promoters such that the addition of D-amino acids to the animals'

drinking water activates DAAO in target tissues, thereby increasing cellular $H_2O_2$ and causing oxidative stress (10, 11). Studies of these "transgenic/chemogenetic" mouse lines have facilitated the analysis of pathways whereby oxidative stress influences disease pathogenesis, and led to the development of novel animal models of neurodegeneration and heart failure caused by tissue-specific chemogenetic oxidative stress in neurons (11) and cardiac myocytes (10), respectively. Here we focus on studies using the DAAO-TG$^{Tie2}$ mouse, in which DAAO is expressed under control of the endothelial cell-specific Tie2 promoter, aiming to define the effects of endothelial cell-specific oxidative stress on the development of hypertension and aortic aneurysms.

Aortic aneurysms are focal enlargements in the lumen of the aorta and represent a major cause of morbidity and mortality in patients (15) (16) (17). There are marked difference in the natural history and risk factors for aortic aneurysms arising in the thoracic aorta (starting at the aortic valve and ending at the diaphragm) versus the abdominal aorta (from the diaphragm to the aortic bifurcation). These two aortic regions have distinct embryological origins and are subject to different hemodynamic forces (18), and different clinical risk factors affect the development of abdominal and thoracic aneurysms (17, 19, 20). Pathological oxidative stress has been implicated in the development of both thoracic and abdominal aorta aneurysms, yet the molecular mechanisms underlying the regional differences in aneurysm formation are incompletely understood. Our current studies of the DAAO-TG$^{Tie2}$ mouse establish that vascular oxidative stress is necessary but not sufficient for aneurysm formation and identify the molecular pathways that underly the differential responses of abdominal versus thoracic aorta to endothelial oxidants.

## RESULTS

### The chemogenetic/transgenic DAAO-TG$^{Tie2}$ mouse line

We generated a chemogenetic transgenic mouse line that express DAAO (D-amino acid oxidase) in vascular endothelial cells to study the effects of chronic oxidative stress on the vasculature. DAAO-TG$^{LoxP}$ mice (11) were crossed with a mouse line expressing Cre recombinase under control of the endothelium-specific Tie2 promoter (Jackson Labs). Founder lines were isolated to create the DAAO-TG$^{Tie2}$ mouse line (Supplemental Figures 1A,B). The Tie2 promoter has been characterized: this promoter is highly active in vascular endothelial cells, but there is also some Tie2 promoter-driven transgene expression in hematopoietic cells(21, 22).

### Effects of chronic oxidative stress on D-alanine-fed DAAO-TG$^{Tie2}$ mice

In our previous studies of transgenic mice expressing DAAO in cardiac myocytes (10) or sensory neurons(11), we found that D-alanine treatment produced a striking disease phenotype within a few days or weeks of treatment. As we had done previously, we provided DAAO-TG$^{Tie2}$ transgenic and control mice with 0.75 M D-alanine in their drinking water, and then monitored the animals carefully, anticipating the development of a vascular phenotype (Supplemental Figure 1C). All measurements were determined by observers blinded to treatment and genotype. We used two different controls: we studied a *genetic control,* comparing transgene-positive DAAO-TG$^{Tie2}$-mice with their transgene-negative Cre$^{+}$ (Cre$^{+}$/TG$^{-}$) littermates, both of which were fed D-alanine (Figure 1A). We also performed a *treatment control,* in which DAAO-TG$^{Tie2}$ mice were treated either with D-alanine or L-alanine (Figure 1B). For the first two months of treatment, the animals appeared to be healthy and weekly blood pressure measurements (tail cuff) and aortic sonography showed no change. However, following two months of treatment, we observed marked increases in systolic blood pressure (Figure 1C) and in the diameter of the abdominal aorta (Figure 1D) in the DAAO-TG$^{Tie2}$ mice that had been provided with D-alanine, with no change in the diameter of

their thoracic aorta (Figure 1E). In all control animals, the systolic blood pressure and aortic dimensions remained unchanged. After 3 months, we observed a sharp decline in the survival of DAAO-TG$^{Tie2}$ mice subjected to D-alanine treatment; control mice remained viable and healthy (Figure 1). The development of aneurysmal dilatation of the abdominal aortic and the onset of hypertension showed a similar time course (Figure 1F). The D-alanine-fed DAAO-TG$^{Tie2}$ mice appeared healthy, and then died suddenly after 3 months; necropsies performed on D-alanine-fed DAAO-TG$^{Tie2}$ mice revealed that in each case (n=16) the abdominal cavity was filled with blood, suggestive of a vascular catastrophe.

**Comparison of transgene expression in abdominal and thoracic aorta**

A trivial explanation for the difference in aneurysm formation between thoracic and abdominal aorta is that there is differential expression of the DAAO-TG$^{Tie2}$ transgene between these two vascular beds. We stained vascular tissues from transgenic and control mice with antibodies against GFP, which detects the YFP component of the HyPer biosensor in the DAAO-TG$^{Tie2}$ transgenic fusion construct. We found that the transgene is expressed at similar levels in abdominal (Figure 2A) and thoracic aorta (Figure 2B), despite the marked difference in the abdominal aortic dimensions over time following D-alanine treatment. Histopathological staining documented the presence of aortic aneurysms only in the infrarenal portion of the abdominal aorta but not in the thoracic aorta (Figures 2C,2D; Supplemental Figures 2A,2B). Thinning and bulging of the abdominal aortic wall was revealed by elastin staining (Figure 2E,2F; Supplemental Figure 2A,2B) with an increased abdominal lumen circumference in treated DAAO-TG$^{Tie2}$ compared to treated controls (Supplemental Figure 2C). Aortic sonography identified aneurysm formation (> 50% increase in aortic diameter) only in the infrarenal abdominal aorta (Figure 2C) in D-alanine-fed DAAO-TG$^{Tie2}$ mice; male and female mice were affected equally (Supplemental Table 1). The thoracic aorta showed no signs of aneurysm formation in D-alanine-fed DAAO-TG$^{Tie2}$ mice

(Figure 2D, Supplemental Figure 2D, Supplemental Videos 1 and 2). Levels of $H_2O_2$ formation in aortic tissues were analyzed using the Amplex Red Assay (23) either in D-alanine-fed or in untreated DAAO-TG$^{Tie2}$ mice (Supplemental Figure 3A). D-alanine feeding caused an increase in the Amplex Red signal in both thoracic and abdominal aorta in D-alanine-fed DAAO-TG$^{Tie2}$ mice compared to untreated mice, but there was no difference in the Amplex Red signal comparing thoracic versus abdominal aorta. Levels of transgene protein expression were analyzed in immunoblots, and showed no differences between thoracic and abdominal aortae (Supplemental Figure 3B). Fibrosis, elastin degradation and extracellular matrix degradation were documented in the abdominal but not thoracic aorta using histochemical stains (Supplemental Figure 4). We also performed immunostaining in abdominal aortic tissues from D-alanine-treated DAAO-TG$^{Tie2}$ mice using antibodies against a range of "inflammatory" cells, including: CD3 (to detect T cells); CD45 (B cells); CD11c (dendritic cells); CD68 (monocytes); F4/80 (macrophages) and Ly6C (neutrophils). None of the antibodies identified any increase in these inflammatory cells in the aorta analyzed after 3 months of D-alanine feeding (Supplemental Figure 5).

**Bone marrow transplantation experiments to differentiate hematopoietic vs. endothelial cell expression of the Tie2-driven transgene in aortic aneurysm formation**

The "endothelial cell-specific" Tie2 promoter also drives gene expression in hematopoietic cells (21, 22). We irradiated DAAO-TG$^{Tie2}$ and Cre$^{+}$/TG$^{-}$ control mice to ablate hematopoietic cells, and performed bone marrow transplants from non-irradiated donor mice, and then treated the transplant recipients with D-alanine (Supplemental Figure 6A). Bone marrow transplanted from untreated DAAO-TG$^{Tie2}$ mice into irradiated control littermates did not result in any vascular phenotype in wild-type transplant recipients treated with D-alanine (Supplemental Figures 6B,C). By contrast, ablation of bone marrow in DAAO-TG$^{Tie2}$ mice did not prevent the subsequent development of abdominal aortic aneurysms in response to D-alanine feeding after transplantation of bone marrow

177 from unirradiated control mice. (Supplemental Figure 6D). We conclude that expression of the
178 Tie2-driven DAAO transgene in vascular endothelial cells and not in hematopoietic cells, is
179 responsible for the vascular phenotype.
180
181 **Oxidative stress in the abdominal and thoracic aorta**
182 Having observed aneurysm formation in abdominal but not thoracic aorta (Figure 1) despite similar
183 levels of transgene expression (Figure 2), we next explored whether these two aortic regions
184 differed in the levels of oxidative stress induced by D-alanine feeding. Figure 3 shows the results
185 of staining for a range of oxidation markers in sections of abdominal aorta vs. thoracic aorta,
186 quantitating the staining pattern seen for D-alanine-fed DAAO-TG$^{Tie2}$ transgenic versus control
187 mice. Figures 3A and 3B show representative tissue immunostaining for detection of carbonylated
188 proteins (24). Abdominal and thoracic aorta showed similar degree of staining in D-alanine-fed
189 DAAO-TG$^{Tie2}$ mice (Figures 3A, 3B), indicating similar increases in protein carbonylation
190 throughout the vascular wall in abdominal and thoracic aortas– both of which show significant
191 increases in staining compared to D-alanine-fed wild-type controls. Panels 3C and 3D show the
192 results of immunostaining using antibodies against 4-hydroxynonenal (a marker of lipid
193 peroxidation), which reveal a significant increase in lipid peroxidation in the vascular wall in both
194 abdominal and thoracic aorta following D-alanine feeding of DAAO-TG$^{Tie2}$ mice compared to
195 controls- but again without significant differences between the abdominal and thoracic aorta.
196 Similar results are seen when staining for oxidized nucleic acids: Panels 3E and 3F show the results
197 of immunostaining abdominal and thoracic aortic sections using antibodies against 8-
198 hydroxyguanosine, which reveal a marked increase in nucleic acid oxidation following D-alanine
199 feeding of DAAO-TG$^{Tie2}$ mice- yet again without significant differences between abdominal and
200 thoracic aorta. Staining with antibodies against 3-chlorotyrosine (Panels 3G and 3H) to detect
201 protein oxidation yielded similar results as seen with the other markers for oxidative stress shown

above, indicating that generation of $H_2O_2$ in vascular endothelium in D-alanine-fed DAAO-TG$^{Tie2}$ mice leads to similar increases of oxidation throughout the vascular wall for both abdominal and thoracic aorta. All these immunohistochemical markers for oxidation of biomolecules were significantly and similarly increased in abdominal and thoracic aorta from D-alanine fed DAAO-TG$^{Tie2}$ mice, indicating that the oxidative stress is similar in both vascular beds (Figures 3C – 3H). By contrast, quantitative histomorphometry of abdominal and thoracic aorta showed significant decreases in wall thickness only in the abdominal aorta (Figure 3I), while the thickness of the thoracic aorta remained unchanged in DAAO-TG$^{Tie2}$ mice vs. controls (Figure 3J). We quantitated elastin breaks in aortic sections prepared from DAAO-TG$^{Tie2}$ mice and found marked increases in elastin breaks in abdominal but not thoracic aorta following D-alanine feeding (Figures 3K and 3L). Taken together, these observations indicate that the abdominal and thoracic aorta have similar levels of DAAO-TG$^{Tie2}$ transgene expression and oxidative stress throughout the vascular wall, yet only the abdominal aorta undergoes aneurysm formation- along with thinning and disruption of the vascular wall. We therefore turned to proteomic analyses to identify the differential features of the vascular proteome in thoracic vs. abdominal aorta in response to oxidative stress.

**Proteomic analysis of thoracic and abdominal aorta**

We treated DAAO-TG$^{Tie2}$ and control mice with D-alanine for three months, and processed the tissues for proteomic analyses (25). Fold changes in protein abundance were calculated from peptide intensity values, as previously described (26). We detected ~1100 proteins that had quantitatively significant peptide intensity values. In control animals, there was no difference in the proteomic profile between the thoracic and abdominal aorta. But proteomic analyses of thoracic and abdominal aorta isolated from D-alanine-fed DAAO-TG$^{Tie2}$ mice (n=3 for each condition) revealed an increase in 516 proteins in abdominal aorta compared to the thoracic aorta and a decrease in ~500 proteins; 38 proteins were unchanged in abundance. We performed

quantitative proteomic analyses using tandem mass tags (TMT)(27), comparing abdominal aortic samples from DAAO-TG$^{Tie2}$ (n = 3) and control mice (n= 3) after D-alanine feeding. We found no changes in the levels of anti-oxidant enzymes in these proteomic analyses nor any change in levels of nitric oxide synthases. The comparative proteomic findings were complemented by quantitative proteomic analyses (27), which identified ~7000 annotated proteins in the abdominal aorta. These protein sets were ranked according to their quantification value and underwent further analyses to identify the pathways involved in the differential response to oxidative stress.

**Gene set enrichment analysis (GSEA) reveals processes involved in abdominal aneurysm formation**

Quantified proteins were ranked using Gene Set Enrichment Analysis (GSEA)(28, 29) to identify the differentially enriched pathways and biological processes (BP) in the abdominal aorta from D-alanine-treated DAAO-TG$^{Tie2}$ animals compared to controls. These analyses revealed that the four most significantly enriched pathways were associated with aneurysm-related processes in the abdominal aorta. The most striking positive enrichments in the abdominal aorta of D-alanine-treated DAAO-TG$^{Tie2}$ animals were for proteins that are associated either with endothelial-mesenchymal transition (EnMT) (Figure 4A) or with MAPK pathway activation (Figure 4B), which have previously been implicated in aneurysm formation[22-25]. We also found that proteins involved in collagen degradation (Figure 4C) and oxidative phosphorylation (Figure 4D) showed significant positive and negative enrichment, respectively. These findings suggest an increase in processes involved in aneurysm formation (increased collagen degradation) accompanied by the development of redox imbalance (decreased oxidative phosphorylation) in abdominal aorta from D-alanine-treated DAAO-TG$^{Tie2}$ mice.

**Gene ontology biological process (GO:BP) and network analyses implicate VSMC phenotypic switching**

The identification of endothelial-mesenchymal transition (EnMT, Figure 4A) by Gene Set Enrichment Analysis provides a critical clue in the biological effects of oxidative stress in the abdominal aorta. EnMT has been identified as a key determinant for VSMC phenotypic switching and aortic aneurysm formation (30) (31–34). We use the term "phenotypic switching" to refer generally to the transition from contractile to synthetic phenotypes, which can occur in response to diverse stimuli. We therefore performed Gene Ontology Biological Process (GO:BP) analysis (35) within the EnMT gene set to get further insight into the aneurysm-related biological processes in this model (the EnMT gene set is in Supplemental Table 2). GO:BP analysis identified enriched processes related to VSMC phenotypic switching: D-alanine treatment of DAAO-TG$^{Tie2}$ animals caused a switch from the "contractile" vascular smooth muscle phenotype found in control aortas to be replaced by a "synthetic" VSMC phenotype in which contractile proteins are lost and markers of fibrosis appear (36–38)(Figure 4E).

Phenotypic switching of VSMCs has been identified as a fundamental process in the pathogenesis of aortic aneurysms (38, 39). The enrichment of EnMT process identified in the proteomic studies (Figure 4A) indicates that abdominal aortic VSMCs in D-alanine-treated DAAO-TG$^{Tie2}$ animals have undergone a phenotypic change. By contrast, proteomic analyses of thoracic aorta did not show any enrichment of EnMT pathways. There is complete concordance between the tissue phenotypes (Figures 2, 3) and the proteomic signatures of abdominal and thoracic aorta from D-alanine treated DAAO-TG$^{Tie2}$ mice (Figures 3, 4). To identify the principal regulators of the EnMT network (Figure 4F), we performed dynamic degree centrality analysis of the network (40, 41). Degree centrality values of different proteins in a network reflect the connectivity and importance of the different proteins that are expressed in a biological system, permitting the identification of

the key regulatory hubs of that specific protein network. Our centrality measurements identified a subset of abdominal aorta proteins as the central regulatory nodes of the EnMT network in the aorta of D-alanine-treated DAAO-TG$^{Tie2}$ mice. These proteins include collagen-1A1, α-smooth muscle actin, and other structural proteins seen in the VSMC extracellular matrix and in synthetic VSMCs. Of all these proteins, Collagen-1A1 was identified as the single central hub of this network (Figure 4G and Supplemental Table 3).

After observing that VSMC phenotypic switching occurs in the abdominal aorta because of D-alanine treatment in DAAO-TG$^{Tie2}$ mice (Figures 3, 4), we compared the abdominal and thoracic proteomic datasets to determine whether VSMC in both of these aortic regions underwent phenotypic switching. Comparative proteomics of abdominal and thoracic aorta indicated increased abundance of mesenchymal VSMC marker (CD34) and the fibroblast VSMC markers (Col1a1, Dcn, Fn1, Cnn1) in D-alanine-treated DAAO-TG$^{Tie2}$ abdominal aorta but not in thoracic aorta (Figure 4H). We also observed a significant decrease in contractile proteins (α-SMA/Acta2, Myh11, Tgln3) only in the abdominal aorta of D-alanine-fed DAAO-TG$^{Tie2}$ mice, indicating a shift from a "contractile" to a "synthetic" VSMC phenotype (42) (Figure 4H). Quantitation of the proteins in the EnMT dataset following GSEA analysis were plotted as a heat map with reference to the abdominal and thoracic proteome dataset (Figure 4I; Supplemental Figure 7A). Taken together, these observations indicate that VSMCs of the abdominal aorta but not thoracic aorta undergo phenotypic switching in response to chronic oxidative stress. These regional findings in proteomic profiles comparing abdominal and thoracic aorta in D-alanine-treated DAAO-TG$^{Tie2}$ animals exactly parallel the differences seen in the abdominal aorta when comparing transgenic and control animals fed D-alanine.

**Identification of JNK1 as the central regulator of VSMC phenotype switching**

We next analyzed the quantitative abdominal aorta proteomic dataset using GO:BP analyses (35) and reactome pathway analyses to identify the most important proteins and interactions involved in the response to chemogenetic oxidative stress. These analyses identified the MAP kinase activation cascade (GO:0000165; $p<0.001$) as the single most significantly enriched processes (Supplemental Tables 4 and 5). We focused on the MAP kinase subcluster from the quantitative proteomic dataset to identify central regulatory nodes. Degree centrality analysis of the MAP kinase subcluster indicated that the MAP kinase signaling protein JNK1 is the central hub of this network, implicating JNK1 as the central regulator of the MAP kinase pathway that is altered in the abdominal aorta of D-alanine-fed DAAO-TG$^{Tie2}$ mice (Figure 5A). Analyses of centrality scores (40, 41) (degree centrality, Eigen factor centrality) for this network then identified the MAP kinase pathway signaling proteins ASK1, MEK7 and DUSP3 as the key determinants of JNK1 activity (Figures 5B and 5C; Supplemental Table 6). We again used Gene Ontology: Biological Process (GO:BP) analysis to identify the critical biological processes enriched in the JNK1 network (Figure 5D). Our analysis identified a significant enrichment of processes related to oxidative stress; regulation of JNK cascade; and VSMC phenotypic switching (Figure 5D; Supplemental Figure 8A and Supplemental Table 7). Many of these processes have been previously implicated in aneurysmal pathophysiology (17, 37, 38, 43), and our current proteomic findings identify a link between the JNK1 cascade and VSMC phenotypic switching.

We hypothesized that oxidant-modulated signaling proteins might play a key role in activating the MAP kinase cascade, and we noted that the MAP kinase family member ASK1 (Apoptosis Signal-regulated Kinase-1) undergoes auto-phosphorylation when it becomes oxidized (44–46). The abundance of key proteins involved in the GO:BP enrichments compared between abdominal aorta from control and D-alanine treated DAAO-TG$^{Tie2}$ mice indicated a significant and striking increase

in the level of DUSP3 (Supplemental Figure 8B), a phosphoprotein phosphatase that dephosphorylates JNK1 and leads to a marked decrease in JNK1 activity (47–49). Since the protein levels of the three key MAPKs involved in JNK1 regulation (ASK1, MEK7, JNK1) were unchanged (Supplemental Figure 8B), we speculated that the observed increase in DUSP3 abundance in aorta of D-alanine-treated DAAO-TG$^{Tie2}$ mice (Supplemental Figure 8B) might lead to an increase in DUSP3-mediated dephosphorylation of JNK1, thereby leading to a decrease in JNK1 activity and the nuclear translocation of KLF4. We tested this hypothesis by exploring the pattern of phosphorylation of these MAP kinase signaling proteins in immunoblots probed with phosphospecific antibodies (Figure 6 A and 6 B).

**JNK1 induces VSMC phenotypic switching in abdominal but not in thoracic aorta via the oxidant-modulated protein kinase ASK1**

Since protein abundance level of the key MAP kinases of the cascade did not change, we probed immunoblots with phosphospecific antibodies for ASK1 and its downstream MAP kinases, which revealed major changes in the phosphorylation status of ASK1 and two other key signaling proteins involved in the MAP kinase signaling cascade (Figure 6A). We used phosphospecific antibodies for ASK1, MEK7 and JNK1 to probe immunoblots of abdominal and thoracic aorta from control and DAAO-TG$^{Tie2}$ mice after 3 months of D-alanine treatment. Both ASK1 and MEK7 showed marked increases in phosphorylation in abdominal and thoracic aorta, while JNK1 showed a striking *decrease* in phosphorylation along with a significant increase in DUSP3 protein level in abdominal aorta compared to thoracic aorta (Figure 6B). These observations suggest that dephosphorylation of JNK1 by DUSP3 in the abdominal aorta leads to JNK1 inactivation, suggesting that JNK1 dephosphorylation by DUSP3 may be a critical determinant of aneurysm formation. JNK1 has been identified as a critical determinant of the nuclear localization of transcription factor KLF4 (50–52). In turn, KLF4 has been identified as a critical determinant in

VSMC phenotypic switching in aneurysm formation. JNK1 phosphorylation inhibits the translocation of KLF4 to the cell nucleus (50). Since JNK1 phosphorylation is decreased in abdominal (but not thoracic) aorta after D-alanine treatment of DAAO-TG$^{Tie2}$ mice, we postulated that nuclear localization of KLF4 would be found in abdominal but not thoracic aorta following D-alanine feeding. Figure 6C and 6D shows the results of immunostaining for KLF4, and reveals that there is a striking increase in KLF4 (Figure 6I) in abdominal aorta of D-alanine-fed DAAO-TG$^{Tie2}$ mice. We next probed for the abundance of two key KLF4 target genes, α-SMA and MYH11, which are important structural proteins in the vascular wall and are markers for contractile VSMC (37, 42). We found that the abdominal aorta has significantly lower abundance of α-SMA and MYH11 compared to thoracic aorta in D-alanine-fed DAAO-TG$^{Tie2}$ mice (Figures 6E, F, G, H). The decrease in α-SMA and MYH11 in the abdominal aorta after D-alanine feeding of DAAO-TG$^{Tie2}$ mice is consistent with a shift from a contractile to synthetic VSMC phenotype because of increased KLF4, which itself is a consequence of dysregulated MAP kinase signaling in response to oxidative stress.

**Effects of DUSP3 inhibition on the vascular pathophenotype**

These studies have suggested a pathway leading from the generation of endothelial $H_2O_2$ in DAAO-TG$^{Tie2}$ mice to yield a striking vascular pathophenotype characterized by systemic hypertension and abdominal aortic aneurysm formation (Figure 7A). A key role for the phosphoprotein phosphatase DUSP3 was suggested both from proteomic (Figure 5B-C) and biochemical analyses (Figure 6A-B). We sought further evidence for the role of DUSP3 by using an in vivo pharmacological approach to test the hypothesis that DUSP3 is a key determinant of the vascular pathophenotype seen after D-alanine feeding of DAAO-TG$^{Tie2}$ mice. We administered the highly specific small molecule DUSP3 inhibitor MLS-0437605 (53) by daily oral gavage (4 mg/kg/day) to DAAO-TG$^{Tie2}$ and control mice at the initiation of D-alanine feeding and continued

375 treatment for 3 months. As shown in Figure 7B, administration of the DUSP3 inhibitor completely
376 blocked the development of abdominal aortic aneurysms in D-alanine-fed DAAO-TG$^{Tie2}$ mice.
377 The DUSP3 inhibitor also markedly attenuated the hypertension caused by D-alanine feeding in
378 DAAO-TG$^{Tie2}$ mice; there was still a small but statistically significant increase in blood pressure
379 in the DUSP3-treated D-alanine-fed DAAO-TG$^{Tie2}$ mice compared to the negative controls (Figure
380 7C).
381
382 **Discussion**
383
384 These studies provide evidence that oxidative stress generated by recombinant D-amino acid
385 oxidase expressed in vascular endothelial cells leads to abdominal aortic aneurysm formation,
386 hypertension, and premature death in DAAO-TG$^{Tie2}$ transgenic mice fed D-alanine (Figures 1,
387 2). Numerous previous reports in multiple animal models have provided evidence that oxidative
388 stress is associated both with hypertension (1) and with the development of aortic aneurysms (8,
389 9). But the complexity and lack of specificity of these aneurysm models (8, 9) has made it difficult
390 to establish that oxidative stress was itself causal. Here we have used chemogenetic approaches to
391 establish that oxidative stress explicitly and specifically causes hypertension and aortic aneurysm
392 formation. Confidence in this conclusion comes from rigorous genetic and treatment control
393 experiments, which confirm that endothelial oxidative stress is necessary for this pathophenotype:
394 neither aortic aneurysms nor hypertension develop in transgene-negative littermates fed D-alanine
395 nor in DAAO-TG$^{Tie2}$ transgenic mice fed L-alanine.
396
397 The formation of abdominal aortic aneurysms and the development of hypertension in DAAO-
398 TG$^{Tie2}$ transgenic mice is observed only after more than two months of D-alanine treatment, and
399 this pathophenotype is not fully expressed until three months of treatment- soon after which point

all the D-alanine-fed transgenic animals die (Figure 1). We focused on characterizing the molecular and cellular features of the aorta at three months of D-alanine feeding, at which point the vascular pathophenotype was uniformly present in DAAO-TG$^{Tie2}$ transgenic mice. We found that vascular smooth muscle cells throughout the abdominal as well as thoracic aorta showed evidence of protein carbonylation (Figures 3A,B), lipid peroxidation (Figures 3C,D), nucleic acid oxidation (Figures 3E,F) and protein tyrosine chlorination (Figures 3G,H). While expression of the DAAO transgene is limited to the vascular endothelium (Figure 2), markers of oxidative stress are seen throughout the vascular wall (Figure 3). Since $H_2O_2$ is a small lipophilic molecule, it is plausible that $H_2O_2$ generated by DAAO in endothelial cells diffuses throughout the vascular wall, causing oxidative modifications in vascular smooth muscle cell proteins, lipids, and nucleic acids. It is also possible that oxidative damage limited to vascular endothelial cells leads to production of chemokines that attract inflammatory cells to the aortic wall, and it is these newly-recruited cells that cause oxidative stress throughout the aortic wall. However, we found no increase in the prevalence of macrophages, neutrophils, dendritic cells, or T cells in the vascular wall of D-alanine-fed DAAO-TG$^{Tie2}$ transgenic mice compared to controls (Supplemental Figure 5). It is still possible that inflammatory cells were present in the aortic wall earlier in the time course of D-alanine feeding but not at the study end point. However, bone marrow transplant experiments established that the vascular phenotype is a result of transgene expression in endothelial cells, not in hematopoietic cells. It is possible that other experimental approaches (e.g. single-cell RNA sequencing) could provide further clues into alterations of the cellular composition of the aorta in response to oxidative stress. In any event, our data indicate that activation of the DAAO transgene in vascular endothelial cells is the critical proximal cause of the pathophenotype.

Despite evidence for similar levels of oxidative stress throughout the abdominal and thoracic aortic walls of D-alanine-fed DAAO-TG$^{Tie2}$ transgenic mice, only the abdominal aorta shows evidence

425 of wall thinning (Figures 3I,J) and elastin breaks (Figures 3K,L) and only the abdominal aorta
426 develops aneurysms leading to premature death (Figure 2). So while oxidative stress is necessary
427 for development of the pathophenotype, *oxidative stress alone is not sufficient*: despite similar
428 levels of transgene expression (Figure 2) and evidence for oxidative stress throughout the length
429 of the aorta (Figure 3), only the abdominal aorta but not the thoracic aorta develops aneurysms.
430 Despite the structural continuity of the aorta along its length, thoracic and abdominal aorta arise
431 from different embryological progenitors (18) and are subjected to different hemodynamic
432 forces(54) (55, 56). Indeed, thoracic and abdominal aortic aneurysms in patients develop in
433 response to different clinical and genetic risk factors, and patients who develop aortic aneurysms
434 have different trajectories of disease progression and variable responses to therapy. The present
435 studies provide proteomic and biochemical evidence indicating that differential signaling
436 responses to vascular oxidants form the basis for differential development of aortic aneurysms in
437 thoracic vs. abdominal aorta despite similar levels of oxidative stress.
438
439 These studies have provided multiple lines of evidence indicating that phenotypic switching is
440 taking place in VSMC of the abdominal but not thoracic aorta in D-alanine-fed DAAO-TG$^{Tie2}$
441 mice. Gene Set Enrichment Analysis (GSEA) of comparative proteomics datasets (Figure 4)
442 documents enrichment of aneurysm-related processes in abdominal aorta in response to oxidative
443 stress. GSEA documents a significant positive enrichment of proteins involved in endothelial-
444 mesenchymal transition (EnMT) (Figure 4A). EnMT has been implicated in aortic aneurysm
445 formation via phenotypic switching of VSMC. These findings establish a causal link between
446 $H_2O_2$-mediated oxidative stress and vascular phenotypic switching in vivo.
447
448 The results of GSEA using comparative proteomics (Figure 4) are complemented and extended by
449 quantitative proteomics analyses (Figure 5), which identified changes in the levels of specific

proteins and their related connectivity networks between abdominal and thoracic aorta in D-alanine-fed DAAO-TG$^{Tie2}$ mice. The MAP kinase signaling pathway, which has been previously implicated in the response to oxidative stress (57) was also identified in these studies. Quantitative proteomics analyses identified the MAP kinase signaling cascade involving JNK1, ASK1, MEK7, and DUSP3 in the pathway involved in VSMC phenotypic switching (Figure 5). The MAP kinase JNK1 was identified as the central node in this pathway, yet the protein abundance of JNK1, ASK1, and MEK7 were unchanged. These findings suggest that changes in the phosphorylation of MAP kinase signaling proteins might be a root cause of the observed phenotypic switching. We noted that the abundance of phosphoprotein phosphatase DUSP3 is much greater in abdominal aorta in comparison to thoracic aorta (Figures 5 and 6). When we probed immunoblots of abdominal and thoracic aorta tissue isolated from D-alanine-fed DAAO-TG$^{Tie2}$ mice with phosphospecific antibodies, we found a marked decrease in JNK1 phosphorylation in the abdominal aorta from D-alanine-fed DAAO-TG$^{Tie2}$ mice. The dephosphorylation of JNK1 by the phosphoprotein phosphatase DUSP3 causes deactivation of JNK1(49). We conclude that JNK1 is a key determinant of the phenotypic switch seen in abdominal aorta of D-alanine-fed DAAO-TG$^{Tie2}$ mice, and this process is critically modulated by the phosphoprotein phosphatase DUSP3, which dephosphorylates and thereby inactivates JNK1. We next asked what are the molecular consequence of the dephosphorylation and inactivation of JNK1 in these cells, and how can this process be connected to VSMC phenotypic switching? Several lines of investigation implicate activation of the JNK1-modulated transcription factor KLF4 as the critical genetic determinant of the phenotypic switch in these cells.

KLF4 is a ubiquitous transcription factor that has been implicated in cellular de-differentiation in a broad range of cell types. There are important connections between JNK1 and KLF4: the nuclear translocation and subsequent activation of KLF4 are suppressed by JNK1. Conversely, inhibition

475 of JNK1 leads to an increase in KLF4 nuclear translocation and the activation of its transcriptional
476 program. We used both immunoblot (Figures 6A,B) and immunohistochemical (Figures 6C-I)
477 approaches to show that dephosphorylation of JNK1 is associated with a striking increase in KLF4
478 in the vascular wall in the abdominal aorta of D-alanine-fed DAAO-TG$^{Tie2}$ mice. This increase in
479 KLF4 is associated with significant decreases in the abundance of alpha-SMA and MYH11
480 (Figures 6G-6I), which are markers of the contractile VSMC phenotype (42), providing direct
481 evidence of phenotypic switching in vascular smooth muscle cells(34, 36, 39, 42, 58).
482
483 These studies have used multiple experimental approaches to identify the proteins and pathways
484 involved in this differential response to oxidative stress in abdominal vs. thoracic aorta. These
485 findings are summarized in a schematic (Figure 8) showing the pathways initiated by the
486 chemogenetic generation of $H_2O_2$ in endothelial cells in the abdominal aorta of D-alanine-fed
487 DAAO-TG$^{Tie2}$ mice. Endothelium-derived $H_2O_2$ (generated by DAAO) activates the oxidant-
488 modulated kinase ASK1 in VSMCs, promoting phosphorylation of the MAP kinase MEK7, which
489 then phosphorylates JNK1- which is the central determinant of phenotypic switching as identified
490 in our proteomic analyses (Figure 5). The MAP kinase phosphatase DUSP3 is expressed in
491 abdominal but not thoracic aorta (Figure 6). We postulate that DUSP3 promotes the
492 dephosphorylation and consequent deactivation of the MAP kinase JNK1, which causes the
493 nuclear translocation of the transcription factor KLF4, which promotes the phenotypic switch from
494 contractile to synthetic vascular smooth muscle cells, leading to vascular wall thinning and
495 aneurysm formation in the abdominal but not thoracic aorta.
496
497 Aortic aneurysms remain a major cause of morbidity and mortality worldwide, and current
498 treatments and preventive strategies have limited efficacy. The present studies may provide a new
499 incentive to explore the use of antioxidant supplements or drugs for the prevention or treatment of

abdominal aortic aneurysms. The effects of antioxidants have not been explicitly studied in patients with abdominal aortic aneurysms(59), and it is plausible that administration of antioxidants might attenuate disease progression in selected patients with abdominal aortic aneurysms. The present studies have implicated the phosphoprotein phosphatase DUSP3 as a critical determinant of abdominal aortic aneurysm formation. The role of DUSP3 in redox metabolism is incompletely understood, but DUSP3 knockout mice show partial attenuation of kidney injury in a model of renal ischemia-reperfusion (60). Recent preclinical studies have explored roles for DUSP3 (61), and other phosphoprotein phosphatase inhibitors are being studied in a broad range of disease states(53, 62–64). Much remains to be learned about the cell-specific pathways that are deranged by reactive oxygen species, but we believe that chemogenetic approaches will continue to identify new pharmacological targets to combat the diverse disease states caused by oxidative stress.

## Methods

### Sex as a biological variable

Our study examined both male and female animals, and similar findings were reported in both sexes

### Mouse models

All the experiments were carried out according to NIH guidelines for the care of laboratory mice, and all animal protocols were approved by the Brigham and Women's Hospital Institutional Animal Care and Use Committee (Protocol 2016N000278). Mice were housed (<5 animals/cage) in cages with regular chow diet (Purina Rodent Diet #5053) and continuous access to drinking water (with D-alanine or L-alanine, as indicated) in a 12 h light-dark cycle. Room temperature was maintained at 21±2°C with 35% humidity. Studies were initiated when the animals were 8 weeks of age. Transgenic animals were developed and characterized as previously described (11).Littermates expressing the Cre recombinase but without the transgene ($Cre^{+}/TG^{-}$) serve as

negative genetic controls. The primer sequences used for genotyping are: Forward: TTCCCTCGTGATCTGCAACTC and reverse: CTTTAAGCCTGCCCAGAAGACT for Rosa26 wild-type; Forward: TTAATCCATATTGGCAGAACGAAAACG and reverse: CAGGCTAAGTGCCTTCTCTACA for recognition of Cre recombinase; and Forward: GGGAGGTGTGGGAGGTTTT and Reverse: CTTTAAGCCTGCCCAGAAGACT for detection of the HyPer-DAAO transgene. All experimental mice were age and sex matched.

**Antibodies**

Primary antibodies used in these studies include: GFP (anti-mouse, Cell Signaling Technology; clone 4B10; catalog# 2955S); vinculin (anti-rabbit, Cell Signaling Technology; clone E1E9V; catalog# 13901S); Phospho-ASK1 (anti-rabbit phospho-Thr 838; Invitrogen; catalog # PA5-64541); ASK1 (anti-rabbit, Cell Signaling Technology; clone D11C9; catalog # 8662S); Acta2 (anti-mouse, Novus biologicals; catalog # NBP2-22120); KLF4 (anti-rabbit, Proteintech; catalog # 11880-1-AP); Myh11 (anti-rabbit, Proteintech; catalog # 21404-1-AP); Phospho-JNK (anti-rabbit, phospho-Thr183/Tyr185) (Cell Signaling Technology; clone 81E11; catalog # 4668S); JNK (anti-rabbit, Cell Signaling Technology; catalog # 9252S); MKK7 (anti-rabbit, Cell Signaling Technology; catalog # 4172S); Phospho-MKK7 (anti-rabbit, phosphor-Ser271/Thr275; Invitrogen; catalog # MA5-28042); DUSP3 (anti-rabbit, Cell Signaling Technology; catalog # 4752S); CD68 (anti-rabbit, Proteintech; catalog # 257471-1-AP); Ly6V/Ly6G (anti-rabbit, Novus Biologicals; catalog # NB600-1387); F4/80 (anti-rabbit, Novus biologicals; catalog #NB600-404SS); CD3E (anti-hamster, R & D solutions; catalog # MAB484); CD45 (anti-rabbit, Cell Signaling Technology; clone 3F8Q; catalog # 70257S); CD11c (anti-rabbit, Cell Signaling Technology; clone D1V9Y; catalog # 97585S); 4-hydroxynonenal (anti-rabbit, Bioss Antibodies; catalog # bs-6313R); 8-hydroxy guanosine (anti-rabbit, Bioss Antibodies; catalog # bs-1278R); 4-chlorotyrosine (anti-rabbit, Hycult; catalog # HP5002-20UG); 4-nitrotyrosine (anti-rabbit,

549 Invitrogen; catalog # A21285); GAPDH (anti-rabbit, Cell Signaling Technology; Clone 14C10;
550 catalog # 2118S).
551 The following secondary antibodies were used for immunofluorescence and immunoblot
552 experiments: Anti-rabbit IgG, HRP conjugated (Cell Signaling Technology; catalog# 7074S); Goat
553 anti-rabbit Alexa 647 (Invitrogen; catalog # A21245); Goat anti-rabbit Alexa 594 (Invitrogen;
554 catalog # A11012); Goat anti-mouse Alexa 488 (Invitrogen; catalog # A11001)
555 **Histology and quantitative histomorphometry**
556 All physiological and imaging analyses were performed by personnel blinded to genotype and/or
557 treatment. Experimental and control animals were anesthetized with isoflurane and perfused with
558 PBS and then with 4% PFA. Abdominal and thoracic aorta were dissected out separately after
559 perfusion and then fixed, embedded in paraffin or OCT, and sectioned. Slides were stained with
560 hematoxylin and eosin, Van Gieson's Elastin stain (EVG), or Masson's Trichrome stain. Images
561 were captured with an Axioskop microscope (ZEISS, Oberkochen, Germany) equipped with a
562 Excelis MPX-20C Camera (Accu-Scope, Commack, NY, USA) and a Achroplan 10X/0.25 Ph1 as
563 well as 40X/0.65 Ph1 objective (ZEISS). Images were captured and analyzed via Capta Vision
564 software (Accu-Scope).
565 For Oxy-IHC, fresh aorta was isolated from mice and fixed overnight with Methacarn (60%
566 methanol, 30% chloroform and 10% glacial acetic acid) at 4°C. Fixed tissues were paraffinized to
567 prepare blocks and slides for sectioning (5 μm). Staining for carbonylated proteins was performed
568 with the oxy-IHC kit (Millipore, USA), and images were quantified using ImageJ.
569 **Immunoblotting**
570 Thoracic and abdominal aortic tissues were collected after animal sacrifice, mechanically
571 dissociated, and then lysed in RIPA lysis buffer (Boston BioProducts, Boston, MA, USA). After
572 lysis, tissue samples were centrifuged at 12000 RPM for 15 min to precipitate tissue debris. Protein

concentration was measured using BCA method (Thermo-Fisher Scientific). Equal amount of protein (20 µg) were mixed with 4x Laemmli buffer (Bio-Rad laboratories), resolved on 10% polyacrylamide gels and transferred to nitrocellulose membranes (Bio-Rad Laboratories). Membranes were washed with TBST (Tris Buffered Saline with 0.1% Tween-20, Boston BioProducts) and blocked with 5% nonfat dry milk in TBST for 1 h. Membranes were incubated at 4°C overnight with primary antibodies and then washed with TBST and incubated with HRP labelled goat anti-rabbit immunoglobulin (Cell Signaling Technology, Danvers, MA, USA). The membranes were washed (3x5 mins) with TBST and developed with enhanced chemiluminescent technique (Super Signal WestFemto, Thermo-Fisher Scientific) and imaged with ChemiDoc™ MP Imaging System (Bio-Rad Laboratories).

**Immunofluorescence**

For immunofluorescence staining, mice were anesthetized, and fresh tissues were collected after intracardiac perfusion, fixed, and sectioned; slides were prepared in paraffin as well as OCT. The sections were deparaffinized, rehydrated and washed in PBS. The sections were blocked with 2% BSA in PBS for 1 h and stained with primary antibodies overnight at 4°C. The next day, sections were washed with PBS and incubated with secondary antibodies for 1 h. Stained sections were observed under Zeiss LSM700 Confocal microscope in x40 and x60 oil immersion objectives and images were captured in Zeiss Zen Black software. Images were analyzed via ImageJ.

Immunofluorescence images for oxidative stress markers were obtained on an inverted microscope (IX80, Olympus, Waltham, MA, USA) equipped with a Lumen 200 Fluorescence Illumination System (Prior, Rockland, MA, USA) and CCD camera (Hamamatsu, Bridgewater, NJ, USA) using a 40x oil immersion objective (UPlanSApo, Olympus). Motorized filter wheels were controlled by a Sutter Lambda 10–3 controller (Sutter Instruments, Novato, CA, USA) and MetaMorph Imaging software version 7.10.5.476 (Molecular Devices LLC., San Jose, CA, USA). Fluorescence of

oxidative markers (HNE, 3-CT and 8-OHG) labelled with goat anti rabbit Alexa 547 secondary antibody were captured using a dichroic filter (SP Gold-B OMF, Semrock). Images were background subtracted and fluorescence intensities were quantified by the Metamorph software. For mouse-on-mouse immunofluorescence staining, the M.O.M immunodetection kit (Vector Laboratories) was used and the staining was carried out according to manufacturer's protocol.

**Blood pressure measurement**

Mice were acclimatized for 1 hour before measuring blood pressure. The readings were taken on 3 consecutive days and the readings of the last day were considered as the final reading and used for further analysis. Blood pressure was measured by tail cuff method (65) with a BP-2000 series II instrument (VisiTech Systems) and measurements were recorded in BP-2000 blood pressure analyzer. The observers were blinded to genotype and to treatment.

**$H_2O_2$ quantification in aortic tissues using the Amplex Red assay**

Thoracic and abdominal aorta were isolated from D-alanine-fed (3 months, 0.75 M) or untreated DAAO-TG$^{Tie2}$ mice. The aortae were cleared of any associated fat or tissue, cut into 2 mm rings, and incubated for 45 mins in Krebs Ringer's Phosphate Glucose (KRPG) buffer pH 7.4 at 37°C. $H_2O_2$ was measured using the Amplex Red assay following the manufacturer's protocols (Life Technologies, Grand Island, NY). Levels of $H_2O_2$ were calculated based on a contemporaneous $H_2O_2$ standard curve and the results presented as pmoles/min/aortic ring.

**DUSP3 inhibitor treatment**

DUSP3 inhibitor (MLS-0437605, or DUSP-I) was from MedChem express (NJ, USA). Four groups of mice were set up for the experiment. A genetic control consisted of Cre$^{+}$/transgene negative mice fed with D-alanine, and a treatment control group studied DAAO-TG $^{Tie2}$ transgenic mice fed L-Ala. The experimental groups were DAAO-TG $^{Tie2}$ transgenic mice, both of which were provided with D-alanine in their drinking water; in one group the DUSP3-inhibitor DUSP3-

622 I was administered by daily oral gavage at a dose of 4 mg/kg/day. There were three mice in each
623 group, and blood pressure and vascular sonography measurements were obtained by observers
624 blinded to genotype and to treatment.

625 **Vascular ultrasonography**

626 Vascular ultrasonography was performed as described (10) using a Visual Sonics F2 system
627 equipped with a UHF57x probe. Treated control and transgenic mice were anesthetized with
628 isoflurane to sustain heart rate above 450 bpm. Standard echocardiographic images of transverse
629 and longitudinal views of abdominal and thoracic aorta were obtained. Images were analyzed with
630 Vevo LAB software (V.3.1.1 FUJIFILM Visualsonics, Toronto, Canada). The sonographer and
631 analyzer were blinded to the experimental treatment and/or genotype. All sonograph images were
632 taken in the diastolic state of the aorta.

633 **Bone-marrow transplantation**

634 Wild type (n=3) and DAAO-TG$^{Tie2}$ (n=3) mice were gamma irradiated (11 Gy in 2 exposures; 5.5
635 Gy each) for 15 min. DAAO-TG$^{Tie2}$ bone marrow (n=3) was injected into irradiated wild type
636 mice, and wild type bone marrow (n=3) was injected into irradiated DAAO-TG$^{Tie2}$ mice via tail
637 vein injection. The mice were provided with 0.75 M D-Ala water along with antibiotics for 3
638 months. Aortic sonography was performed on the mice every two weeks for 3 months to observe
639 aneurysm formation.

640 **Proteomic analyses of aortic tissues**

641 Fresh thoracic and abdominal aorta tissues were collected separately from control (n=3) and
642 transgenic mice (n=3) and homogenized in RIPA lysis buffer. Total protein was TCA precipitated
643 and resolubilized in RapigestSF (Waters). Resolubilized proteins were reduced with DTT (10 mM
644 30 mins 80°C) and alkylated with iodoacetamide (20 mM, 30 min at room temperature). 2 ml of
645 modified sequencing-grade trypsin (20 ng/ml) (Promega, Madison, WI) was added to each sample

and the samples were placed in a 37ºC water bath overnight. Before proteomic analyses, samples were acidified by adding 20 µl 20% formic acid solution and then desalted using a C18 STAGE tip.

LC-MS analyses followed established protocols (11, 25). On the day of analysis, the samples were reconstituted in 10 µl of HPLC solvent A (66). A reverse-phase HPLC capillary column was created by packing C18 spherical silica beads into a silica capillary. Each sample was loaded via a Famos auto sampler (LC Packings, San Francisco CA). A gradient was formed, and peptides were eluted with increasing concentrations of solvent B (97.5% acetonitrile, 0.1% formic acid). Eluted peptides were subjected to electrospray ionization and then passed through an LTQ Orbitrap Velos Elite ion-trap mass spectrometer (Thermo Fisher Scientific, Waltham, MA). Peptides were detected, isolated, and fragmented to produce a tandem mass spectrum of specific fragment ions for each peptide. Peptide sequences were determined by matching protein databases with the acquired fragmentation pattern by the software program, Sequest (Thermo Fisher Scientific, Waltham, MA). All databases include a reversed version of all the sequences and the data was filtered to reduce the peptide false discovery rate to 1-2%.

The label-free quantification values of the annotated proteins were normalized by $\log_2$ transformation. Pairwise comparison between group was done by t-test and one way ANOVA using GraphPad Prism 9. Differences according to Benjamin- Hochberg adjusted p value $<0.05$ were considered significant.

**TMT labelling and quantitative proteomic analyses**

Samples for quantitative protein analysis were prepared as previously described (67). Proteins were extracted from aortic tissues using urea lysis buffer (Roche). Following tissue lysis, 25 µg of each protein was reduced with 5 mM TCEP. Cysteine residues were alkylated using 10 mM iodoacetamide. Excess iodoacetamide was quenched with 10 mM DTT. A buffer exchange was

carried out using a modified SP3 protocol (66). Samples were digested overnight at room temperature. The next morning trypsin was added to each sample and incubated for 6 hours at 37º C. Acetonitrile was added to each sample to a final concentration of ~33%. Each sample was labelled in the presence of SP3 beads, with ~62.5 µg of TMTpro reagents (ThermoFisher Scientific) and then desalted via Stage Tips and re-dissolved in 5% formic acid/ 5% acetonitrile for LC-MS3 analysis via a Orbitrap Mass spectrometer.

Raw files were converted to mzXML, and monoisotopic peaks were re-assigned using Monocle (68). Searches were performed using the Comet search algorithm against a mouse database downloaded from Uniprot in May 2021. We used a 50 ppm precursor ion tolerance, 1.0005 fragment ion tolerance, and 0.4 fragment bin offset for MS2 scans collected in the ion trap. TMTpro on lysine residues and peptide N-termini (+304.2071 Da) and carbamidomethylation of cysteine residues (+57.0215 Da) were set as static modifications, while oxidation of methionine residues (+15.9949 Da) was set as a variable modification. Each run was filtered separately to 1% False Discovery Rate (FDR) on the peptide-spectrum match (PSM) level, as described(27, 67).

**Proteomic data analysis**

Gene set enrichment analysis (GSEA) of proteomics datasets of comparative abdominal-thoracic proteome and quantitative abdominal aorta proteome were performed on preranked annotated protein set as described(29) against reference MsigDB database. P value <0.05 and FDR value <0.25 was considered significant for the analysis(28).

Networks were created with Rpackage “igraph” and degree centrality analysis was carried out by Gephi supported R package “rgexf”. Networks were visualized with CytoscapeR. R package “go.db” was used for GO:BP enrichment analysis of annotated proteome with DAVID based annotated GO terms (*Mus musculus*)as reference. Pathway analysis of annotated proteins was performed using R package “clusterProfiler” against mice Reactome pathway database. Heatmaps

were created using R package Complex Heatmap (version 2.10.0). Bar graphs and histograms were built in GraphPad Prism 9.

**Statistical analysis**

Statistical analysis for in-between group comparisons was performed using Student's t-test (for two group comparisons) or two-way ANOVA with appropriate post-testing (for ≥3 group comparisons). Data values are presented as individual data points and expressed as means ± standard error of mean (SEM). Individual statistical tests are described in the corresponding figure legends. A P value of $< 0.05$ was considered statistically significant. Equal numbers of male and female mice were studied. All physiological, and imaging studies performed and analyzed by scientists blinded to genotype and treatment. Statistical analyses were performed using GraphPad Prism 9.0 (GraphPad Software, La Jolla, CA).

**Study Approval**

All the experiments were carried out according to NIH guidelines for the care of laboratory mice, and all animal protocols were approved by the Brigham and Women's Hospital Institutional Animal Care and Use Committee (Protocol 2016N000278).

**Data Availability**

All data are available in the manuscript, supplemental data files and supporting data values. Raw proteomic data was submitted to PRIDE repositories (PXD060700,PXD060737)

**Author Contributions:**

AD, MWW, FS, SY, AP, TD, and TC designed and performed experiments, and were involved in experimental design and interpretation along with TM. TM and AD wrote the manuscript.

**Acknowledgements:**

This study was supported by National Institutes of Health (NIH) grants R33 HL157918, R21 AG063073 and R01 HL152173 to T.M.; NIH grant K08 HL168240 to F.S.; FWF 21 fellowship award J4466-B to M.W.W. We appreciate the engagement of Matteo Sabatine and Ryan Wolf in pilot experiments. T.C. was supported by a LaDue Fellowship from Harvard Medical School.

## References

1. Griendling KK, et al. Oxidative Stress and Hypertension. Circ Res. 2021;128(7):993–1020.
2. Madamanchi NR, Vendrov A, Runge MS. Oxidative Stress and Vascular Disease. Arterioscler Thromb Vasc Biol. 2005;25(1):29–38.
3. Emeto TI, et al. Oxidative stress and abdominal aortic aneurysm: potential treatment targets. Clin Sci. 2016;130(5):301–315.
4. Chen Q, et al. Reactive oxygen species: key regulators in vascular health and diseases. Br J Pharmacol. 2018;175(8):1279–1292.
5. Camargo LL, et al. Reactive oxygen species in hypertension. Nat Rev Cardiol. [published online ahead of print: July 24, 2024]. https://doi.org/10.1038/s41569-024-01062-6.
6. Ushio-Fukai M, et al. Interplay Between Reactive Oxygen/Reactive Nitrogen Species and Metabolism in Vascular Biology and Disease. Antioxid Redox Signal. 2021;34(16):1319–1354.
7. Porto FG, et al. Evidence for a protective role of Protein Disulfide Isomerase-A1 against aortic dissection. Atherosclerosis. 2023;382:117283.
8. Lysgaard Poulsen J, Stubbe J, Lindholt JS. Animal Models Used to Explore Abdominal Aortic Aneurysms: A Systematic Review. European Journal of Vascular and Endovascular Surgery. 2016;52(4):487–499.
9. Trollope A, et al. Animal models of abdominal aortic aneurysm and their role in furthering management of human disease. Cardiovascular Pathology. 2011;20(2):114–123.
10. Spyropoulos F, et al. Adult and neonatal models of chemogenetic heart failure caused by oxidative stress. Journal of Clinical Investigation. 2024;134(9). https://doi.org/10.1172/JCI178251.
11. Yadav S, et al. Sensory ataxia and cardiac hypertrophy caused by neurovascular oxidative stress in chemogenetic transgenic mouse lines. Nat Commun. 2023;14(1):3094.
12. Waldeck-Weiermair M, et al. Dissecting in vivo and in vitro redox responses using chemogenetics. Free Radic Biol Med. 2021;177:360–369.
13. Spinelli JB, et al. Metabolic recycling of ammonia via glutamate dehydrogenase supports breast cancer biomass. Science. 2017;358(6365):941–946.
14. Matlashov ME, Belousov V V., Enikolopov G. How Much $H_2O_2$ Is Produced by Recombinant D-Amino Acid Oxidase in Mammalian Cells? Antioxid Redox Signal. 2014;20(7):1039–1044.

15. Isselbacher EM, et al. 2022 ACC/AHA Guideline for the Diagnosis and Management of Aortic Disease: A Report of the American Heart Association/American College of Cardiology Joint Committee on Clinical Practice Guidelines. Circulation. 2022;146(24). https://doi.org/10.1161/CIR.0000000000001106.
16. Ito S, et al. Embryonic Heterogeneity of Smooth Muscle Cells in the Complex Mechanisms of Thoracic Aortic Aneurysms. Genes (Basel). 2022;13(9):1618.
17. Sakalihasan N, et al. Abdominal aortic aneurysms. Nat Rev Dis Primers. 2018;4(1):34.
18. Majesky MW. Developmental Basis of Vascular Smooth Muscle Diversity. Arterioscler Thromb Vasc Biol. 2007;27(6):1248–1258.
19. Chou E, et al. Genetics and mechanisms of thoracic aortic disease. Nat Rev Cardiol. 2023;20(3):168–180.
20. Pinard A, Jones GT, Milewicz DM. Genetics of Thoracic and Abdominal Aortic Diseases. Circ Res. 2019;124(4):588–606.
21. Arai F, et al. Tie2/Angiopoietin-1 Signaling Regulates Hematopoietic Stem Cell Quiescence in the Bone Marrow Niche. Cell. 2004;118(2):149–161.
22. Ito K, et al. Self-renewal of a purified Tie2 $^{+}$ hematopoietic stem cell population relies on mitochondrial clearance. Science (1979). 2016;354(6316):1156–1160.
23. Parastatidis I, et al. Overexpression of Catalase in Vascular Smooth Muscle Cells Prevents the Formation of Abdominal Aortic Aneurysms. Arterioscler Thromb Vasc Biol. 2013;33(10):2389–2396.
24. Smith CD, et al. Excess brain protein oxidation and enzyme dysfunction in normal aging and in Alzheimer disease. Proceedings of the National Academy of Sciences. 1991;88(23):10540–10543.
25. Rappsilber J, Ishihama Y, Mann M. Stop and Go Extraction Tips for Matrix-Assisted Laser Desorption/Ionization, Nanoelectrospray, and LC/MS Sample Pretreatment in Proteomics. Anal Chem. 2003;75(3):663–670.
26. Schwanhäusser B, et al. Global quantification of mammalian gene expression control. Nature. 2011;473(7347):337–342.
27. Li J, et al. TMTpro-18plex: The Expanded and Complete Set of TMTpro Reagents for Sample Multiplexing. J Proteome Res. 2021;20(5):2964–2972.
28. Subramanian A, et al. Gene set enrichment analysis: A knowledge-based approach for interpreting genome-wide expression profiles. Proceedings of the National Academy of Sciences. 2005;102(43):15545–15550.
29. Mootha VK, et al. PGC-1α-responsive genes involved in oxidative phosphorylation are coordinately downregulated in human diabetes. Nat Genet. 2003;34(3):267–273.
30. Miano JM, Fisher EA, Majesky MW. Fate and State of Vascular Smooth Muscle Cells in Atherosclerosis. Circulation. 2021;143(21):2110–2116.
31. Coll-Bonfill N, et al. Transdifferentiation of endothelial cells to smooth muscle cells play an important role in vascular remodelling. Am J Stem Cells. 2015;4(1):13–21.
32. Kovacic JC, et al. Endothelial to Mesenchymal Transition in Cardiovascular Disease. J Am Coll Cardiol. 2019;73(2):190–209.
33. Kovacic JC, et al. Epithelial-to-Mesenchymal and Endothelial-to-Mesenchymal Transition. Circulation. 2012;125(14):1795–1808.
34. Cao G, et al. How vascular smooth muscle cell phenotype switching contributes to vascular disease. Cell Communication and Signaling. 2022;20(1):180.
35. Kolberg L, et al. gprofiler2 -- an R package for gene list functional enrichment analysis and namespace conversion toolset g:Profiler. F1000Res. 2020;9:709.
36. Chen R, et al. Phenotypic Switching of Vascular Smooth Muscle Cells in Atherosclerosis. J Am Heart Assoc. 2023;12(20). https://doi.org/10.1161/JAHA.123.031121.

808 37. Quintana RA, Taylor WR. Cellular Mechanisms of Aortic Aneurysm Formation. Circ Res.
809 2019;124(4):607–618.
810 38. Rombouts KB, et al. The role of vascular smooth muscle cells in the development of aortic
811 aneurysms and dissections. Eur J Clin Invest. 2022;52(4):e13697.
812 39. Lu H, et al. Vascular Smooth Muscle Cells in Aortic Aneurysm: From Genetics to
813 Mechanisms. J Am Heart Assoc. 2021;10(24). https://doi.org/10.1161/JAHA.121.023601.
814 40. Jeong H, et al. Lethality and centrality in protein networks. Nature. 2001;411(6833):41–42.
815 41. Yang Y, Dong Y, Chawla N V. Predicting Node Degree Centrality with the Node Prominence
816 Profile. Sci Rep. 2014;4(1):7236.
817 42. Yap C, et al. Six Shades of Vascular Smooth Muscle Cells Illuminated by KLF4 (Krüppel-
818 Like Factor 4). Arterioscler Thromb Vasc Biol. 2021;41(11):2693–2707.
819 43. Mack CP. Signaling Mechanisms That Regulate Smooth Muscle Cell Differentiation.
820 Arterioscler Thromb Vasc Biol. 2011;31(7):1495–1505.
821 44. Hattori K, et al. The roles of ASK family proteins in stress responses and diseases. Cell
822 Communication and Signaling. 2009;7(1):9.
823 45. Morales Betanzos C, et al. Dynamic Phosphorylation of Apoptosis Signal Regulating Kinase
824 1 (ASK1) in Response to Oxidative and Electrophilic Stress. Chem Res Toxicol.
825 2016;29(12):2175–2183.
826 46. Tobiume K, Saitoh M, Ichijo H. Activation of apoptosis signal-regulating kinase 1 by the
827 stress-induced activating phosphorylation of pre-formed oligomer. J Cell Physiol.
828 2002;191(1):95–104.
829 47. Todd JL, et al. Dual-specificity protein tyrosine phosphatase VHR down-regulates c-Jun N-
830 terminal kinase (JNK). Oncogene. 2002;21(16):2573–2583.
831 48. Pavic K, Duan G, Köhn M. <scp>VHR</scp> / <scp>DUSP</scp> 3 phosphatase: structure,
832 function and regulation. FEBS J. 2015;282(10):1871–1890.
833 49. Ha J, et al. Phosphorylation Dynamics of JNK Signaling: Effects of Dual-Specificity
834 Phosphatases (DUSPs) on the JNK Pathway. Int J Mol Sci. 2019;20(24):6157.
835 50. Yao K, et al. JNK1 and 2 play a negative role in reprogramming to pluripotent stem cells by
836 suppressing Klf4 activity. Stem Cell Res. 2014;12(1):139–152.
837 51. Semba T, et al. JNK Signaling in Stem Cell Self-Renewal and Differentiation. Int J Mol Sci.
838 2020;21(7):2613.
839 52. Amand M, et al. DUSP3/VHR is a pro-angiogenic atypical dual-specificity phosphatase. Mol
840 Cancer. 2014;13(1):108.
841 53. Musumeci L, et al. Dual-Specificity Phosphatase 3 Deficiency or Inhibition Limits Platelet
842 Activation and Arterial Thrombosis. Circulation. 2015;131(7):656–668.
843 54. Pande RL, Beckman JA. Pathophysiology, Epidemiology, and Prognosis of Aortic
844 Aneurysms. Vascular Medicine: A Companion to Braunwald's Heart Disease. Elsevier;
845 2013:457–470.
846 55. Mutlu O, et al. How does hemodynamics affect rupture tissue mechanics in abdominal aortic
847 aneurysm: Focus on wall shear stress derived parameters, time-averaged wall shear stress,
848 oscillatory shear index, endothelial cell activation potential, and relative residence time. Comput
849 Biol Med. 2023;154:106609.
850 56. Milewicz DM, et al. Altered Smooth Muscle Cell Force Generation as a Driver of Thoracic
851 Aortic Aneurysms and Dissections. Arterioscler Thromb Vasc Biol. 2017;37(1):26–34.
852 57. Li X, et al. Oxidative Stress–Induced JNK1/2 Activation Triggers Proapoptotic Signaling and
853 Apoptosis That Leads to Diabetic Embryopathy. Diabetes. 2012;61(8):2084–2092.
854 58. Badran A, et al. Reactive Oxygen Species: Modulators of Phenotypic Switch of Vascular
855 Smooth Muscle Cells. Int J Mol Sci. 2020;21(22). https://doi.org/10.3390/ijms21228764.

59. Miller FJ, et al. Oxidative Stress in Human Abdominal Aortic Aneurysms. Arterioscler Thromb Vasc Biol. 2002;22(4):560–565.
60. Khbouz B, et al. The genetic deletion of the Dual Specificity Phosphatase 3 (DUSP3) attenuates kidney damage and inflammation following ischaemia/reperfusion injury in mouse. Acta Physiologica. 2022;234(2). https://doi.org/10.1111/apha.13735.
61. Ríos P, et al. Dual-Specificity Phosphatases as Molecular Targets for Inhibition in Human Disease. Antioxid Redox Signal. 2014;20(14):2251–2273.
62. Guo M, et al. Targeting phosphatases: From molecule design to clinical trials. Eur J Med Chem. 2024;264:116031.
63. Khbouz B, et al. The Dual-specificity Phosphatase 3 (DUSP3): A Potential Target Against Renal Ischemia/Reperfusion Injury. Transplantation. [published online ahead of print: April 8, 2024]. https://doi.org/10.1097/TP.0000000000005009.
64. Monteiro LF, et al. DUSP3/VHR: A Druggable Dual Phosphatase for Human Diseases. Rev Physiol Biochem Pharmacol. 2019;176:1–35.
65. Wilde E, et al. Tail-Cuff Technique and Its Influence on Central Blood Pressure in the Mouse. J Am Heart Assoc. 2017;6(6). https://doi.org/10.1161/JAHA.116.005204.
66. Hughes CS, et al. Single-pot, solid-phase-enhanced sample preparation for proteomics experiments. Nat Protoc. 2019;14(1):68–85.
67. Navarrete-Perea J, et al. Streamlined Tandem Mass Tag (SL-TMT) Protocol: An Efficient Strategy for Quantitative (Phospho)proteome Profiling Using Tandem Mass Tag-Synchronous Precursor Selection-MS3. J Proteome Res. 2018;17(6):2226–2236.
68. Rad R, et al. Improved Monoisotopic Mass Estimation for Deeper Proteome Coverage. J Proteome Res. 2021;20(1):591–598.
69. Filiberto AC, et al. Endothelial pannexin-1 channels modulate macrophage and smooth muscle cell activation in abdominal aortic aneurysm formation. Nat Commun. 2022;13(1):1521.

# Figure legends

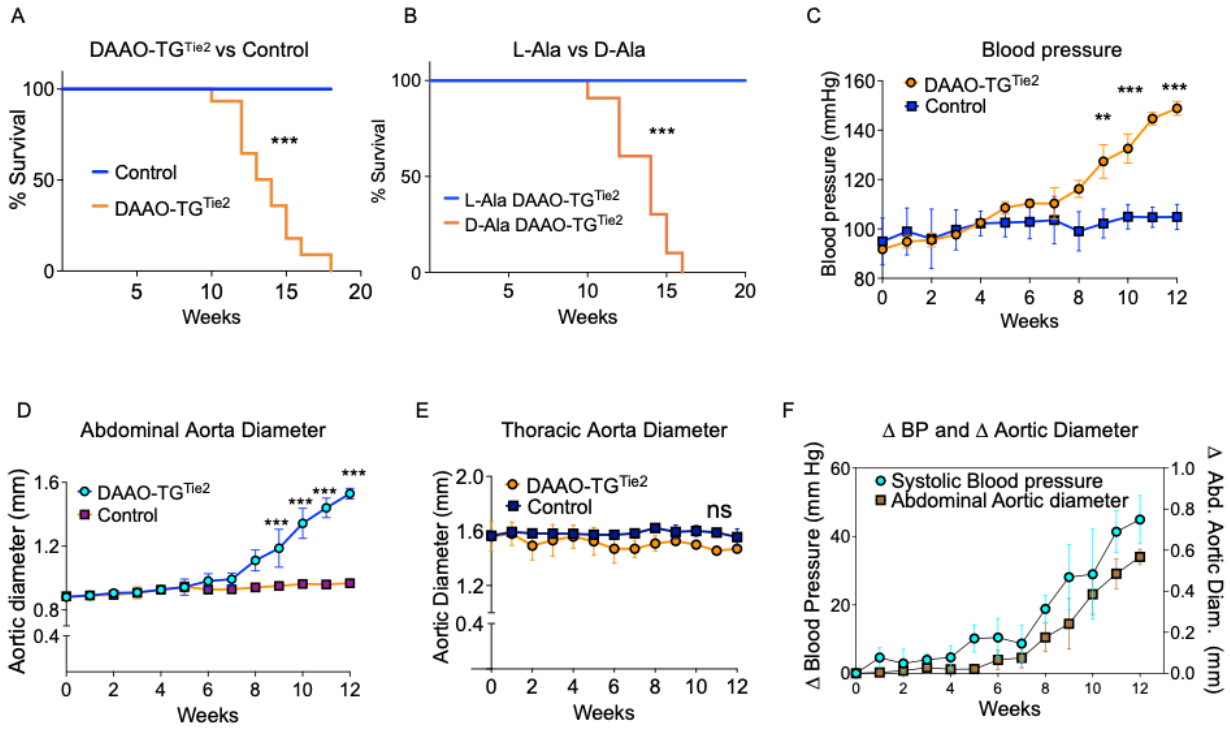


**Figure 1: Effects of chemogenetic oxidative stress on mortality and vascular pathology in DAAO-TG$^{Tie2}$ transgenic mice**

**Panels A and B** show Kaplan-Meier survival curves for DAAO-TG$^{Tie2}$ and control mice exposed to chemogenetic oxidative stress. **Panel A** shows the survival curve for D-alanine-fed DAAO-TG$^{Tie2}$ transgenic mice (blue line), with their wild-type D-alanine-fed littermates serving as negative (genetic) controls (orange line). **Panel B** shows a treatment control in which DAAO-TG$^{Tie2}$ transgenic mice are fed either D-alanine (blue line) or L-alanine (orange line). Chronic D-alanine-fed DAAO-TG$^{Tie2}$ transgenic mice show a drastically reduced survival compared either to their D-alanine-fed wild-type control littermates ($p<0.001$ by ANOVA) or to L-alanine-fed transgenic littermates ($p<0.001$). **Panel C** shows results of systolic blood pressure measurements in DAAO-TG$^{Tie2}$ transgenic (blue line) and their wild-type littermates (orange line) following the initiation of D-alanine-feeding; there is no change in blood pressure until 8 weeks of age, at which

907 point blood pressure increased significantly (** designates $p<0.01$; *** indicates $p<0.001$;
908 ANOVA). Measurements of aortic diameter (determined by sonography) in D-alanine-fed DAAO-
909 $TG^{Tie2}$ transgenic mice (blue line) and their wild-type littermates (orange line) are shown for the
910 abdominal aorta **(panel D)** and the thoracic aorta **(panel E)**. In the DAAO-$TG^{Tie2}$ transgenic mice,
911 the abdominal ($p<0.001$) but not thoracic aortae increase in size following chronic D-alanine
912 feeding. **Panel F** shows a time course plotting the change in systolic blood pressure and the change
913 in abdominal aorta dimensions following the initiation of D-alanine feeding in DAAO-$TG^{Tie2}$
914 transgenic animals compared to wild-type littermate controls; changes in blood pressure and
915 abdominal aortic dimension followed similar time courses. All measurements were made by
916 observers blinded to genotype and treatment. All mice were on a similar C57BL/6 genetic
917 background. The data are presented as the means ± SEM of at least 3 independent experiments.

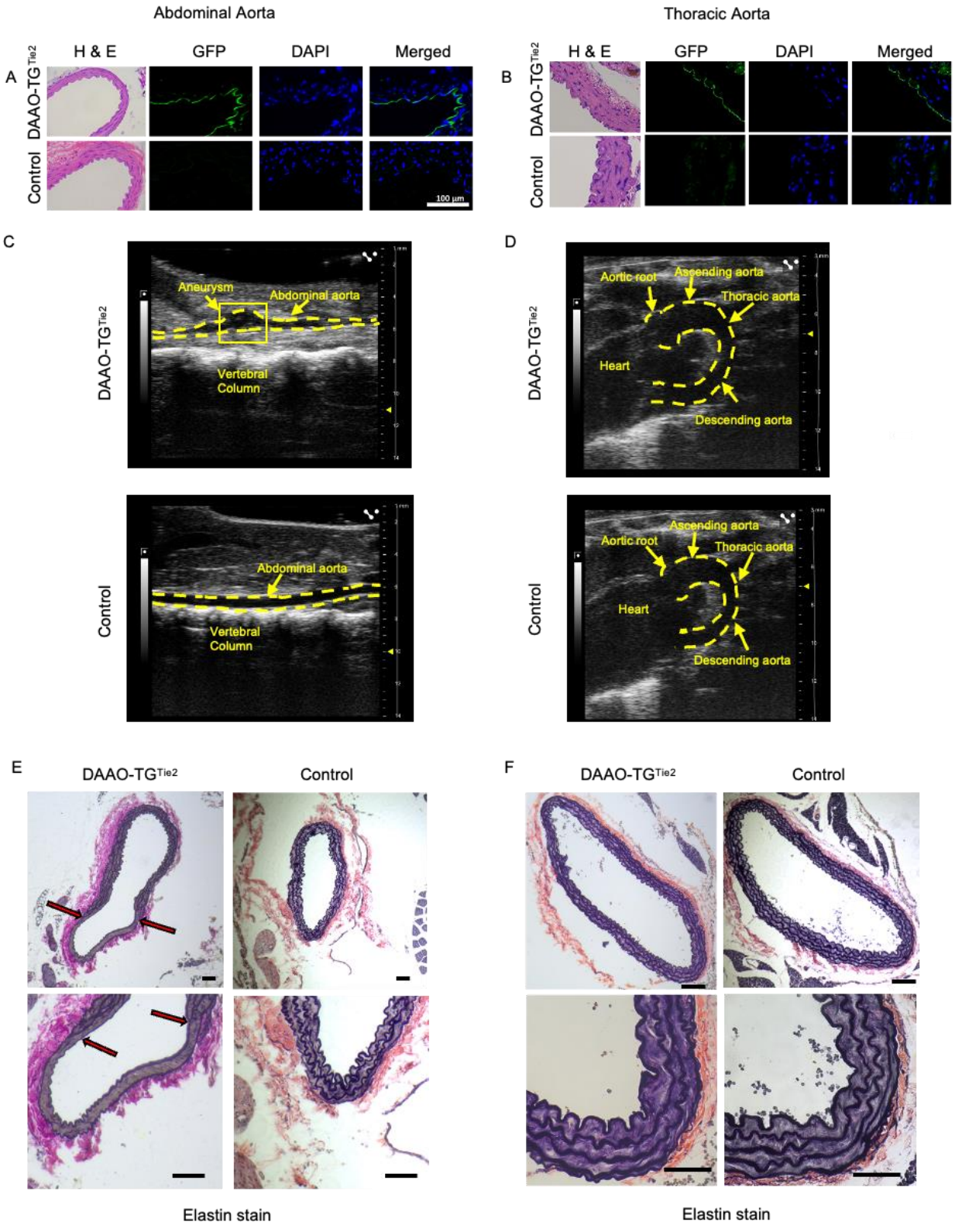
Abdominal Aorta
Thoracic Aorta
A
B
H & E
GFP
DAPI
Merged
DAAO-TG Tie2
Control
100 µm
C
D
Aneurysm
Abdominal aorta
Vertebral Column
Aortic root
Ascending aorta
Thoracic aorta
Heart
Descending aorta
E
F
DAAO-TGTie2
Control
Elastin stain

**Figure 2: Imaging of the abdominal and thoracic aorta following chemogenetic oxidative stress.**

This figure shows representative images of abdominal **(Panels A, C, E)** and thoracic **(Panels B, D, F)** aortae from DAAO-TG$^{Tie2}$ transgenic and control mice. In panels A and B, aortae were isolated from untreated DAAO-TG$^{Tie2}$ transgenic mice or control littermates, and transverse sections were stained with hematoxylin and eosin (H&E); with antibodies against GFP (which detects the YFP that is part of the transgene); or with DAPI to detect cell nuclei. The final panel in each row shows the merged image of GFP and DAPI staining. Expression of the transgene is seen in both abdominal and thoracic aorta in the transgenic mice. Representative aortic sonograms are shown for infrarenal abdominal **(panel C)** and thoracic **(panel D)** aorta from D-alanine-fed DAAO-TG$^{Tie2}$ transgenic and control mice. The dotted lines in each image show the border of the aortic lumen, revealing an aneurysm in abdominal (infrarenal) but not thoracic aorta. The aortic root and the ascending and descending part of the thoracic aorta are denoted by arrows. **Panels E and F** show images of abdominal **(E)** and thoracic **(F)** aortae from D-alanine treated DAAO-TG$^{Tie2}$ or control mice. Fixed aortic sections from were stained with Van Gieson's elastin stain ("Elastin stain"); the upper and lower panels show lower and higher magnifications, and the scale bar designates 40 μm or 10 μm, respectively. An aortic aneurysm can be seen in the abdominal (infrarenal) but not thoracic aorta (descending) sections. Red arrows indicate start and end of aneurysmal bulge in the corresponding lower and higher resolution images. The images presented in this figure are representative of at least 3 independent experiments.

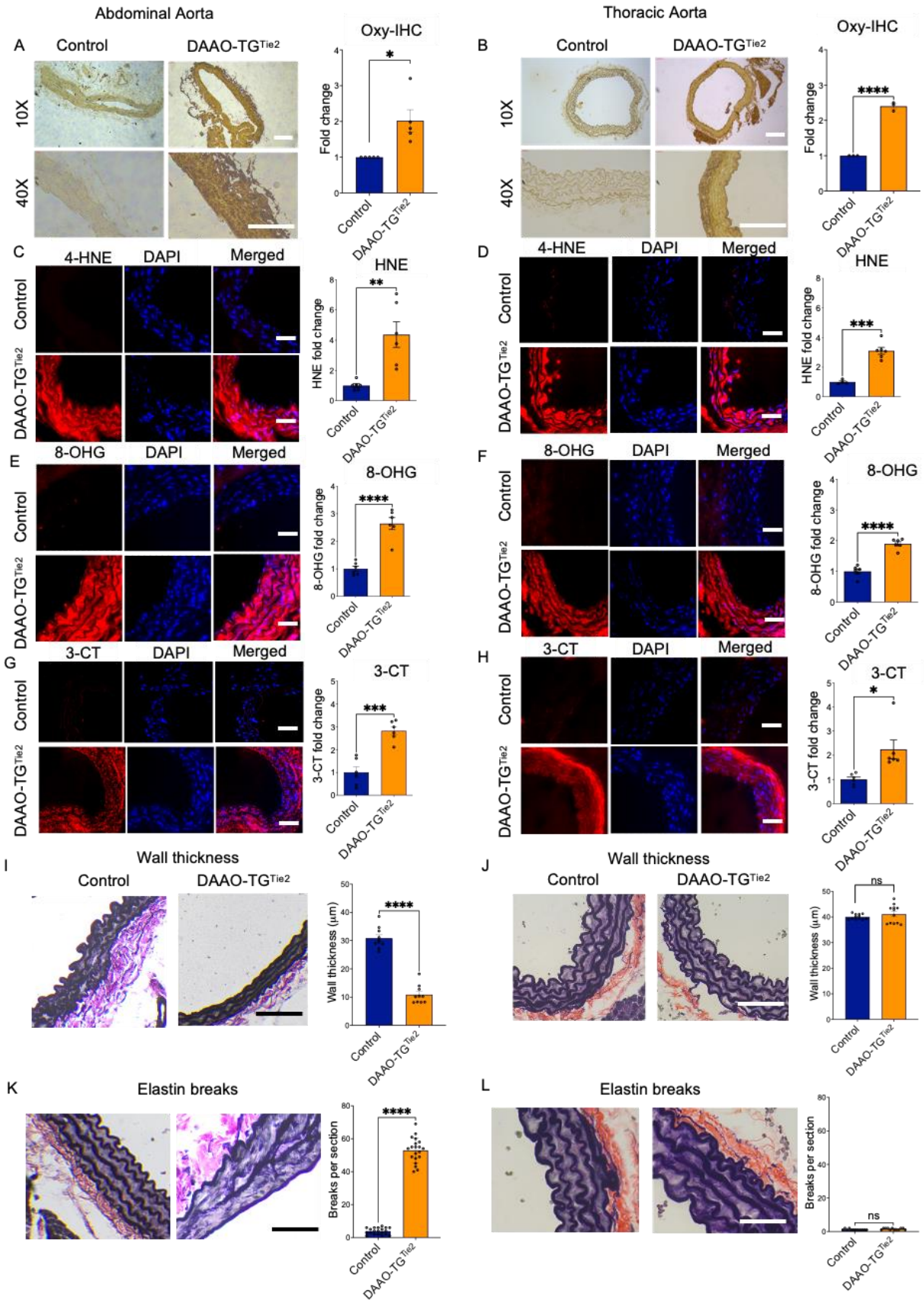
Abdominal Aorta
Thoracic Aorta
A
Control
DAAO-TG^Tie2
10X
40X
Oxy-IHC
Fold change
B
C
4-HNE
DAPI
Merged
HNE
HNE fold change
D
E
8-OHG
8-OHG fold change
F
G
3-CT
3-CT fold change
H
I
Wall thickness
Wall thickness (μm)
J
K
Elastin breaks
Breaks per section
L
ns

944

**Figure 3: Analyses of aortic wall oxidative stress and vessel integrity in abdominal and thoracic aortae isolated from in D-alanine-fed DAAO-TG$^{Tie2}$ transgenic and control mice.** DAAO-TG$^{Tie2}$ transgenic and control mice were treated with D-alanine for two months, and fixed aortic preparations were isolated and analyzed to quantitate markers of oxidative stress and vessel integrity. Throughout this figure, images from abdominal aorta are shown in the panels on the left **(Panels A, C, E, G, I, K)** and images from thoracic aorta are presented in the right-hand panels **(Panels B, D, F, H, J, L)**. For each stain, representative images are shown, followed by quantitative analyses of staining intensity performed by operators blinded to genotype and treatment. Results of staining to detect protein carbonylation (Oxy-IHC) are shown in **Panels A and B**; quantitation of Oxy-IHC staining shows similar increases in protein carbonylation in abdominal **(A)** and thoracic **(B)** aorta. In similar fashion, stains for oxidized lipids (HNE, 4-hydroxynonenal); oxidized nucleic acids (8-OHG, or 8-hydoxyguanosine) or tyrosine chlorination (3-CT, or 3-chlorotyrosine) were increased in both the thoracic and abdominal aorta in D-alanine-fed DAAO-TG$^{Tie2}$ transgenic but not control mice. **Panels I-L** show the results of staining with antibodies directed against elastin to determine aortic wall thickness **(I and J)** and to quantitate elastin breaks **(K and L)** as an index of vessel wall integrity (69). Representative images are shown for each, as well as pooled results of quantitative histomorphometry measuring wall thickness and elastin breaks performed by blinded operators. *, **, ***, and **** designate p values less than 0.05, 0.01, 0.005, and 0.001, respectively (Student's t test). Markers of oxidative stress can be seen to increase in both the abdominal and thoracic aorta following D-alanine feeding of the DAAO-TG$^{Tie2}$ transgenic mice **(panels A-H)**. However, only the abdominal aorta shows wall thinning **(panel I)** and elastin breaks **(panel K)** following D-alanine feeding in DAAO-TG$^{Tie2}$ transgenic mice. Scale bars represent 100 μm. The pooled data are presented as means ± SEM of at least 3 independent experiments.

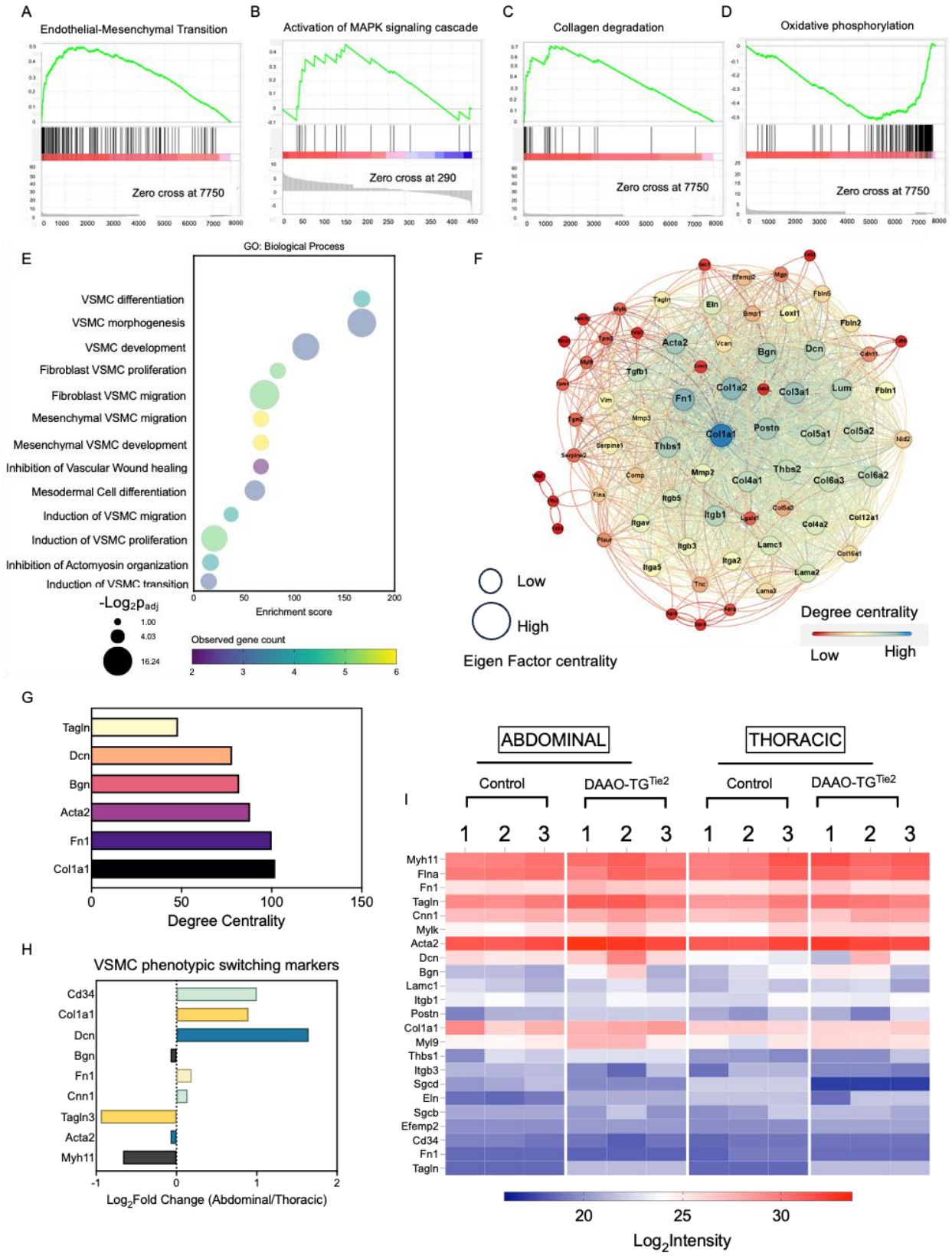
A
Endothelial-Mesenchymal Transition
Zero cross at 7750
B
Activation of MAPK signaling cascade
Zero cross at 290
C
Collagen degradation
Zero cross at 7750
D
Oxidative phosphorylation
Zero cross at 7750
E
GO: Biological Process
VSMC differentiation
VSMC morphogenesis
VSMC development
Fibroblast VSMC proliferation
Fibroblast VSMC migration
Mesenchymal VSMC migration
Mesenchymal VSMC development
Inhibition of Vascular Wound healing
Mesodermal Cell differentiation
Induction of VSMC migration
Induction of VSMC proliferation
Inhibition of Actomyosin organization
Induction of VSMC transition
-Log2padj
1.00
4.03
16.24
Enrichment score
Observed gene count
F
Low
High
Eigen Factor centrality
Degree centrality
Low
High
G
Tagln
Dcn
Bgn
Acta2
Fn1
Col1a1
Degree Centrality
H
VSMC phenotypic switching markers
Cd34
Col1a1
Dcn
Bgn
Fn1
Cnn1
Tagln3
Acta2
Myh11
Log2Fold Change (Abdominal/Thoracic)
I
ABDOMINAL
THORACIC
Control
DAAO-TGTie2
Control
DAAO-TGTie2
1 2 3 1 2 3 1 2 3 1 2 3
Myh11
Flna
Fn1
Tagln
Cnn1
Mylk
Acta2
Dcn
Bgn
Lamc1
Itgb1
Postn
Col1a1
Myl9
Thbs1
Itgb3
Sgcd
Eln
Sgcb
Efemp2
Cd34
Fn1
Tagln
20 25 30
Log2Intensity

969

970

**Figure 4: Proteomic analyses of thoracic and abdominal aorta following chemogenetic oxidative stress**

**Panels A-D** show the results of Gene Set Enrichment Analysis (GSEA) of the TMT proteomics datasets from aortae isolated from D-alanine-fed DAAO-TG$^{Tie2}$ transgenic or control mice subjected to chemogenetic oxidative stress for 3 months. Each of the GSEA (28) shown in panels A-D are characterized by FDR<25% and $p<0.01$. Aortae from D-alanine-fed DAAO-TG$^{Tie2}$ transgenic mice exhibit significantly positive enrichment of pathways involved in endothelial-mesenchymal transition **(Panel A)**; activation of MAPK signaling cascade **(Panel B)**; and collagen degradation **(Panel C)**. **Panel D** shows the markedly negative enrichment of oxidative phosphorylation pathways in the abdominal aorta in D-alanine-fed DAAO-TG$^{Tie2}$ transgenic mice.

**Panel E** is a bubble plot that shows the top Gene Ontology (GO) biological process enrichments from the EnMT reactome gene set (Supplemental Table 2). The enrichment score (on the abscissa) corresponds to the featured biological processes listed along the ordinate. The size of each bubble indicates the $-\log_2 p_{adj}$, and the color of the bubbles indicates the observed gene counts for each of the featured biological processes.

**Panel F** shows the results of centrality analysis for enriched endothelial-mesenchymal (EnMT) pathway proteins shown as an unweighted edge network with proteins shown as nodes and connections as edges. The size of the nodes was scaled on the Eigen factor value, and the color gradient was assigned according to degree centrality scores of each node. The degree centrality is denoted by color as noted in the lookup table, with deep blue showing highest order centrality, and light green showing lowest order centrality. Edge distances were assigned according to closeness centrality(40).

**Panel G** shows a bar graph presenting the degree centrality of the nodes involved in phenotypic switching characterized by having high degree centrality in the Endothelial-Mesenchymal

995 Transition network shown in panel A. The abscissa shows the degree centrality corresponding to
996 the gene names presented along the ordinate.

997 **Panel H** shows a bar graph of significant changes in VSMC phenotypic switching markers in
998 thoracic vs. abdominal aorta based on comparative proteomics data. The abscissa indicates $log_2$
999 fold change of the ratio of abdominal/thoracic values for each marker that corresponds to the
1000 individual VSMC phenotypic switching markers shown along the ordinate.

1001 **Panel I** is a heatmap showing the $Log_2$intensity of all relevant proteins from the EnMT
1002 enrichment dataset (Supplemental Table 2) comparing protein intensity between abdominal and
1003 thoracic aorta from DAAO-$TG^{Tie2}$ transgenic or control mice. The heat map colors represent
1004 $log_2$intensity, with red color indicating higher intensity and blue indicating lower intensity. The
1005 data presented here are representative of the results of at least 3 independent experiments.

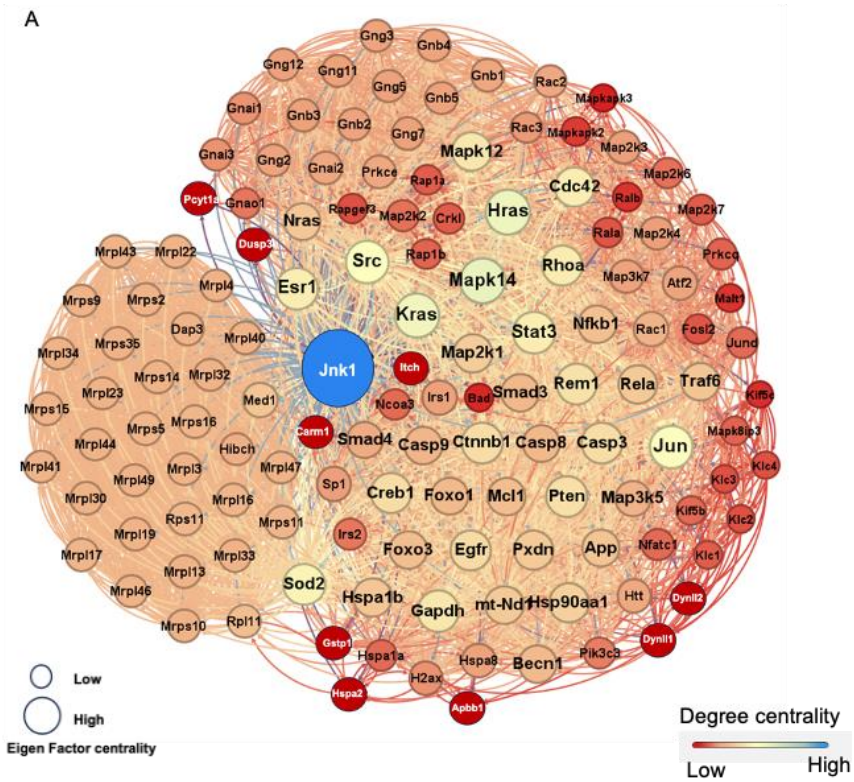
A
Jnk1
Src
Esr1
Mapk14
Mapk12
Cdc42
Hras
Nras
Rhoa
Kras
Rac2
Rac3
Gng3
Gnb4
Gng12
Gng11
Gnb1
Gng5
Gnb5
Gnai1
Gnb3
Gnb2
Gng7
Gnai3
Gng2
Gnai2
Prkce
Rap1a
Pcyt1a
Gnao1
Rapgef3
Map2k2
Crkl
Dusp3
Rap1b
Mrpl43
Mrpl22
Mrpl4
Mrps9
Mrps2
Dap3
Mrpl40
Mrpl34
Mrps35
Mrps14
Mrpl32
Mrpl23
Mrps15
Med1
Mrps5
Mrps16
Mrpl44
Hibch
Mrpl41
Mrpl3
Mrpl47
Mrpl49
Mrpl30
Mrpl16
Rps11
Mrps11
Mrpl19
Mrpl17
Mrpl33
Mrpl13
Mrpl46
Mrps10
Rpl11
Sod2
Hspa1b
Gapdh
mt-Nd1
Hsp90aa1
Htt
Dynll2
Dynll1
Gstp1
Hspa1a
Hspa8
Becn1
Pik3cb
H2ax
Hspa2
Apbb1
Itch
Irs1
Bad
Ncoa3
Carm1
Smad4
Casp9
Ctnnb1
Casp8
Casp3
Jun
Smad3
Rem1
Rela
Traf6
Klf5
Mapk8ip3
Klc4
Klc3
Klf5b
Klc2
Klc1
Nfatc1
Sp1
Creb1
Foxo1
Mcl1
Pten
Map3k5
Irs2
Foxo3
Egfr
Pxdn
App
Mapkapk3
Mapkapk2
Map2k3
Map2k6
Map2k7
Ralb
Rala
Map2k4
Prkcq
Map3k7
Atf2
Malt1
Nfkb1
Rac1
Fosl2
Jund
Map2k1
Stat3
Low
High
Eigen Factor centrality
Degree centrality
Low
High
B
Degree Centrality
300
200
100
0
DUSP3
MEK7
ASK1
JNK1
C
Eigen factor centrality
1.5
1.0
0.5
0.0
DUSP3
MEK7
ASK1
JNK1
D
VSMC phenotypic switching
Dorsal polarity determination
Mesenchymal VSMC differentiation
Oxidative stress induced MAPK cascade
Angiotensin mediated blood pressure
Apical-Basal polarity
VSMC proliferation
Response to H2O2
JNK activity
VSMC stress response
Upregulation of JNK Cascade
Induction of phosphorylation
Fibroblast VSMC proliferation
Downregulation of JNK Cascade
Endothelial-mesenchymal transition
VSMC polarity
VSMC migration
-Log2 padj
4
12
27
Genes Found
1
2
3
4
5
6
9
0
50
100
150
200
Enrichment Score

1006

**Figure 5: Quantitative proteomic analyses of abdominal aorta in D-alanine-treated DAAO-TG$^{Tie2}$ and control mice**

**Panel A** presents the JNK1 protein network and connecting targets identified using quantitative proteomics (27) to compare abdominal aorta in D-alanine-treated DAAO-TG$^{Tie2}$ transgenic and control mice. Node sizes were assigned according to the Eigen factor values, and the colors assigned according to the degree centrality (Blue signifies highest centrality and Red indicates lowest centrality). Edges are unweighted but the distance between two nodes are assigned according to their closeness centrality values. **Panels B and C** show gradient plots of the same data as shown in panel A. **Panel B** shows selected MAPK cascade proteins along the abscissa, with the degree centrality of specific nodes quantitated along the ordinate. **Panel C** is based on the same data as in panel B, but analyzed for Eigen factor centrality for selected MAPK cascade proteins, as shown on the ordinate. **Panel D** shows a "Lollipop Plot" presenting the GO: Biological Processes identified from the same set of proteins used to create panel A. The abscissa presents the enrichment score that corresponds to the enriched biological process listed on the ordinate. The color of the bubbles represents the number of genes identified in each process and the size of the bubbles represents the $-\log_2 p_{adj}$ values, as noted in the lookup table shown to the left of the plot. The data shown in this figure are based on the results of at least 3 independent experiments.

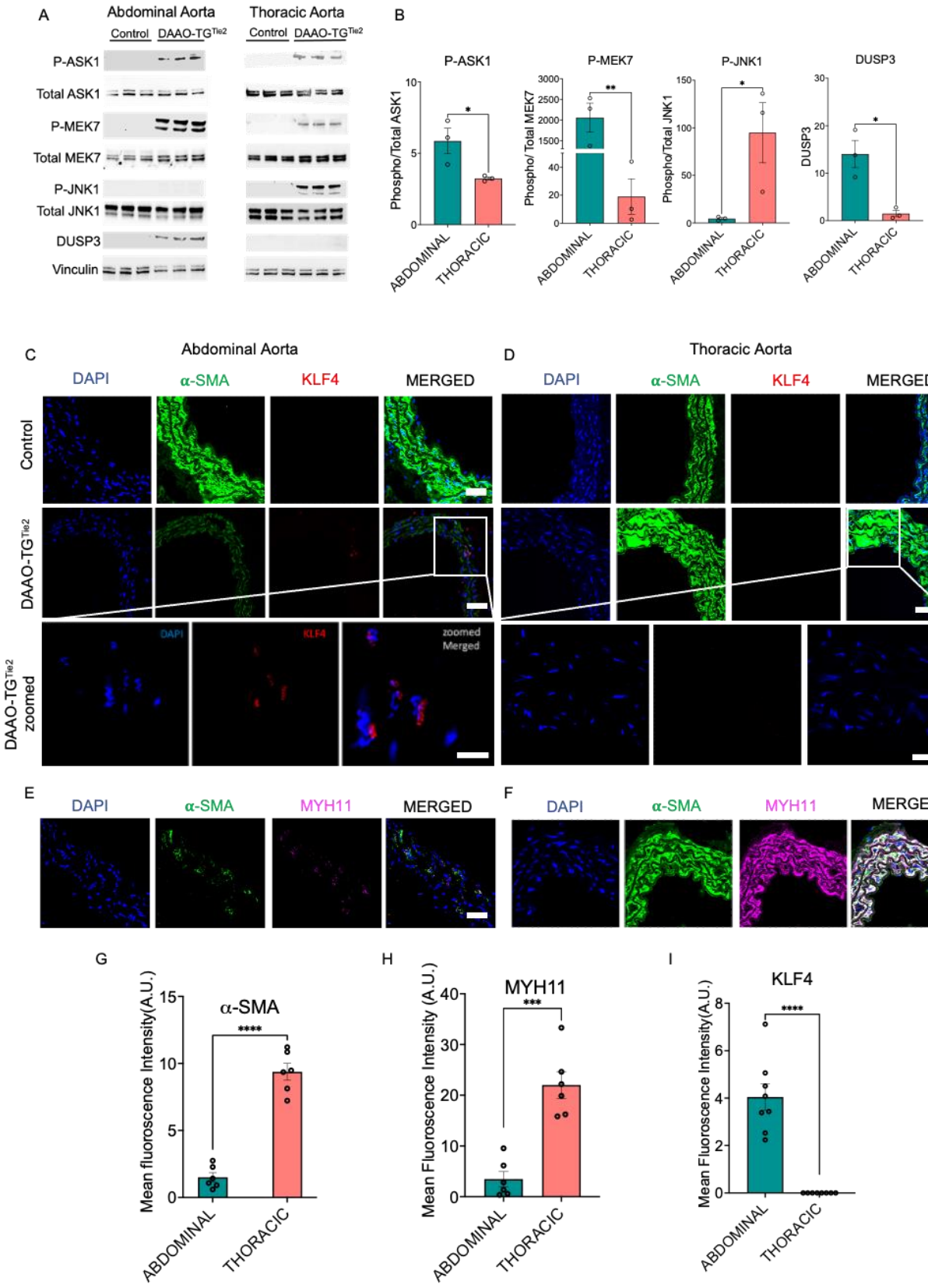
A
Abdominal Aorta
Thoracic Aorta
Control
DAAO-TGTie2
P-ASK1
Total ASK1
P-MEK7
Total MEK7
P-JNK1
Total JNK1
DUSP3
Vinculin
B
P-ASK1
P-MEK7
P-JNK1
DUSP3
Phospho/Total ASK1
Phospho/ Total MEK7
Phospho/Total JNK1
DUSP3
ABDOMINAL
THORACIC
C
Abdominal Aorta
D
Thoracic Aorta
DAPI
α-SMA
KLF4
MERGED
Control
DAAO-TGTie2
DAAO-TGTie2 zoomed
zoomed Merged
E
F
MYH11
G
α-SMA
Mean fluoroscence Intensity(A.U.)
H
MYH11
Mean Fluoroscence Intensity (A.U.)
I
KLF4
Mean Fluoroscence Intensity(A.U.)

**Figure 6: VSMC phenotypic switching in abdominal aorta but not in thoracic aorta.**

**Panel A** show immunoblots probed with phospho-specific or total antibodies directed against three signaling proteins that are critically implicated in VSMC phenotypic switching (36, 42, 58) from the proteomics data: ASK1, MEK7, and JNK1. Each column presents immunoblots probing a single abdominal or thoracic aorta isolated from an individual D-alanine-treated DAAO-TG$^{Tie2}$ transgenic or control mouse. The bar graphs in **panel B** show pooled densitometric quantification data from immunoblots for n=3 mice for each experimental condition; * or ** indicates $p<0.05$ or $p<0.01$, respectively (Student's t test), with vinculin used as a loading control. **Panels C-F** show the results of immunohistochemical staining (40X) in tissue sections isolated from abdominal **(Panels C and E)** or thoracic **(Panels D and F)** aorta from D-alanine-treated or control mice and probed with antibodies as shown. DAPI staining (nuclei) is shown in blue; staining with antibodies against α-SMA and KLF4 is shown in green and red, respectively. The scale bars show 100 μm. The bottom row of images in **Panels C and D** present higher power (60X) views of the same images shown in the row of photomicrographs presented above; the scale bar shows 10 μm. Panel E and F show results of immunohistochemical staining in abdominal **(E)** and thoracic **(F)** aorta sections in D-alanine-fed DAAO-TG$^{Tie2}$ transgenic animals, with antibodies against the synthetic VSMC phenotypic switching markers α-SMA and Myh11(42) shown in green and red, respectively. Pooled data quantitating staining intensity for α-SMA, Myh11, and KLF4 are shown in **Panel G, H, and I**, respectively; *** designates $p<0.001$ and **** indicates $p<0.0001$(Student's t test). Data are presented as means ± SEM of at least 3 independent experiments.

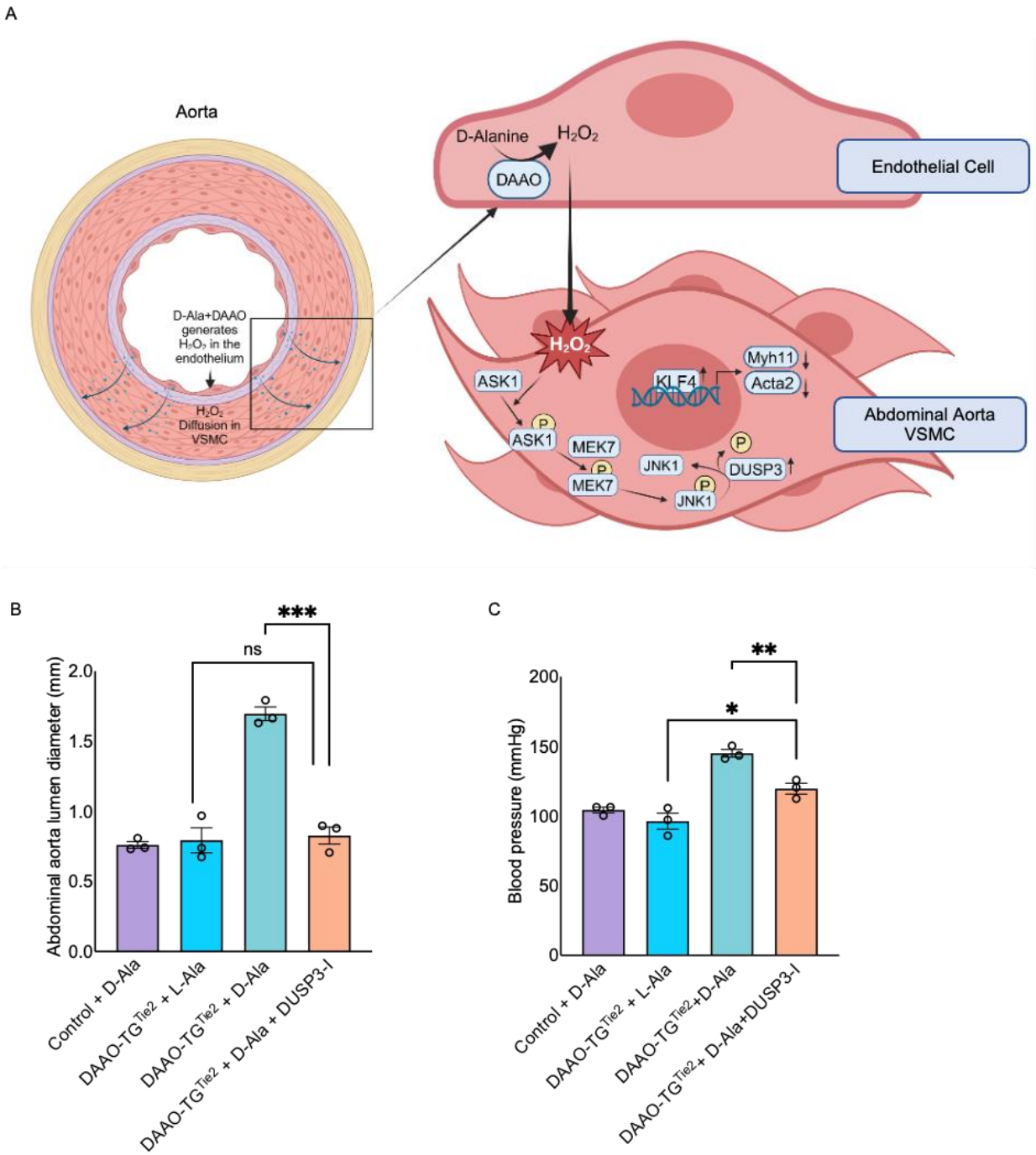


**Figure 7: A key role for DUSP3 in abdominal aortic aneurysm formation caused by oxidative stress.**

The left image in **Panel A** is a schematic showing that hydrogen peroxide generated by DAAO expressed in the vascular endothelium promotes oxidative stress throughout the vascular wall of D-alanine-fed DAAO-TG$^{Tie2}$ transgenic mice (Figure 3). The right image in Panel A shows a

schematic of the signaling pathways initiated by the chemogenetic generation of $H_2O_2$ in vascular endothelial cells that lead ultimately to systemic hypertension and aortic aneurysm formation (Figure 1). Hydrogen peroxide directly promotes ASK1 oxidation and autophosphorylation, which leads to the subsequent phosphorylation of MEK7 and JNK1 (52-57). The phosphoprotein phosphatase DUSP3 is present in abdominal but not thoracic VSMC (Figure 6) and catalyzes the de-phosphorylation of JNK1(49), which is permissive for KLF4 translocation and leads to VSMC phenotypic switching (50).

**Panel B and Panel C** show the vascular phenotype of alanine-fed DAAO-TG$^{Tie2}$ and control mice treated with the small molecule DUSP3 inhibitor MLS-0437605 (DUSP3-I; 4 mg/kg/day by daily oral gavage; REF) for 3 months. The graph on the left (Panel B) presents measurements of abdominal aorta diameter, showing that DUSP3-I treatment completely blocks the formation of aortic aneurysms in D-alanine-fed DAAO-TG$^{Tie2}$ mice. The graph on the right (Panel C) presents systolic blood pressure measurements in control and DAAO-TG$^{Tie2}$ transgenic mice after 3 months of drug + D-alanine treatment, showing that DUSP3-I attenuates the increase in blood pressure seen in the D-alanine fed DAAO-TG$^{Tie2}$ mice that were not treated with DUSP-I. There was a small but statistically significant increase in blood pressure comparing the L-alanine-fed DAAO-TG$^{Tie2}$ and the mice fed D-alanine plus DUSP-I. n=3 mice in each treatment group. ***, **, and * indicate $p<0.001$, $p<0.01$, and $p<0.05$ respectively (Multiple Student's T test and ANNOVA performed for multiple comparisons). Data are presented as means ± SEM of at least 3 independent experiments.

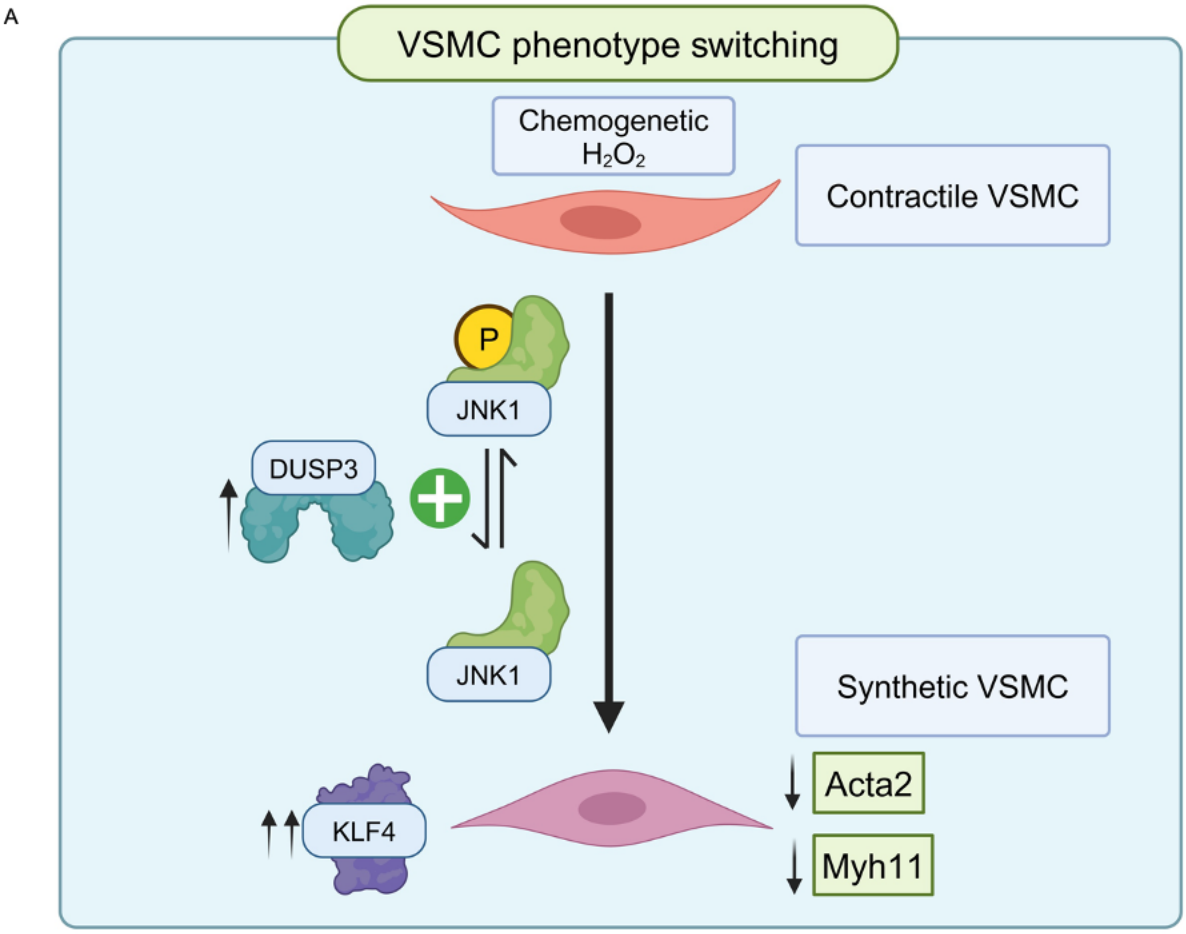


**Figure 8: Schematic of key vascular signaling proteins connecting oxidative stress to phenotypic switching.** This schematic focuses on the phenotypic switch from contractile to synthetic VSMC in the abdominal but not thoracic aorta: dephosphorylation of phosphorylated JNK by the phosphoprotein phosphatase DUSP3 leads to nuclear translocation of the transcription factor KLF4, which causes decreased expression of Acta2 (α-SMA) and Myh11, leading to endothelial-mesenchymal transition and resulting in vascular wall thinning and aneurysm formation in the abdominal aorta.